



UNIVERSITÉ DU
LUXEMBOURG

FACULTY OF SCIENCE, TECHNOLOGY AND COMMUNICATION

The Effect of Noise Level on Causal Identification with Additive Noise Models

Thesis Submitted in Partial Fulfillment of the
Requirements for the Degree of Master in Information
and Computer Sciences

Author:
Benjamin KAP

Supervisor:
Prof. Thomas ENGEL

Reviewer:
Prof. Nicolas NAVET

Advisor:
Dr. Marharyta ALEKSANDROVA

May 2021

Abstract

In recent years a lot of research has been conducted within the area of causal inference and causal learning. Many methods have been developed to identify the cause-effect pairs in models and have been successfully applied to observational real-world data in order to determine the direction of causal relationships. Many of these methods require simplifying assumptions, such as absence of confounding, cycles, and selection bias. Yet in bivariate situations causal discovery problems remain challenging. One class of such methods, that also allows tackling the bivariate case, is based on Additive Noise Models (ANMs). Unfortunately, one aspect of these methods has not received much attention until now: what is the impact of different noise levels on the ability of these methods to identify the direction of the causal relationship. This work aims to bridge this gap with the help of an empirical study. For this work, we considered bivariate cases, which is the most elementary form of a causal discovery problem where one needs to decide whether X causes Y or Y causes X , given joint distributions of two variables X, Y . Furthermore, two specific methods have been selected, *Regression with Subsequent Independence Test* and *Identification using Conditional Variances*, which have been tested with an exhaustive range of ANMs where the additive noises' levels gradually change from 1% to 10000% of the causes' noise level (the latter remains fixed). Additionally, the experiments in this work consider several different types of distributions as well as linear and non-linear ANMs. The results of the experiments show that these methods can fail to capture the true causal direction for some levels of noise.

Contents

Abstract	iii
1 Introduction	1
1.1 State of the Art	1
2 Additive Noise Models and Notation	5
2.1 Experiment Layout	7
3 Experiments on Regression with Subsequent Independence Test	9
3.1 RESIT with Different Noise Levels	9
3.1.1 Setup	10
3.1.2 Execution	15
3.1.3 Experimental Results	15
3.2 RESIT with Different Noise Levels and coupled estimation	27
3.2.1 Results	27
3.3 RESIT with Different Noise Levels without prior assumption	39
3.3.1 Setup	39
3.3.2 Execution	39
3.3.3 Results	39
3.4 RESIT with different means	46
3.4.1 Setup	46
3.4.2 Execution	47
3.4.3 Results	47
4 Experiments on Identification using Conditional Variances	49
4.1 Introduction	49
4.1.1 Algorithm	50
4.2 Setup	52
4.2.1 Execution	52
4.2.2 Results	52
5 Conclusion and Future Work	55

List of Figures

2.1	A simple directed acyclic graph showing causal relationships between variables.	6
2.2	Another directed acyclic graph showing causal relationships between variables.	6
3.1	Data is generated following $Y = X + N_y$ with uniform distributions only. .	12
3.2	RESIT & different noise levels & decoupled estimation & $Y = \mathcal{N} + \mathcal{N}$. .	16
3.3	RESIT & different noise levels & decoupled estimation & $Y = \mathcal{N} + \mathcal{U}$. . .	16
3.4	RESIT & different noise levels & decoupled estimation & $Y = \mathcal{N} + \mathcal{L}$. . .	17
3.5	RESIT & different noise levels & decoupled estimation & $Y = \mathcal{N}^3 + \mathcal{N}$. .	17
3.6	RESIT & different noise levels & decoupled estimation & $Y = \mathcal{N}^3 + \mathcal{U}$. .	18
3.7	RESIT & different noise levels & decoupled estimation & $Y = \mathcal{N}^3 + \mathcal{L}$. .	18
3.8	RESIT & different noise levels & decoupled estimation & $Y = \mathcal{U} + \mathcal{U}$. . .	19
3.9	RESIT & different noise levels & decoupled estimation & $Y = \mathcal{U} + \mathcal{N}$. . .	19
3.10	RESIT & different noise levels & decoupled estimation & $Y = \mathcal{U} + \mathcal{L}$. . .	20
3.11	RESIT & different noise levels & decoupled estimation & $Y = \mathcal{U}^3 + \mathcal{U}$. .	20
3.12	RESIT & different noise levels & decoupled estimation & $Y = \mathcal{U}^3 + \mathcal{N}$. .	21
3.13	RESIT & different noise levels & decoupled estimation & $Y = \mathcal{U}^3 + \mathcal{L}$. .	21
3.14	RESIT & different noise levels & decoupled estimation & $Y = \mathcal{L} + \mathcal{L}$. . .	22
3.15	RESIT & different noise levels & decoupled estimation & $Y = \mathcal{L} + \mathcal{N}$. . .	22
3.16	RESIT & different noise levels & decoupled estimation & $Y = \mathcal{L} + \mathcal{U}$. . .	23
3.17	RESIT & different noise levels & decoupled estimation & $Y = \mathcal{L}^3 + \mathcal{L}$. .	23
3.18	RESIT & different noise levels & decoupled estimation & $Y = \mathcal{L}^3 + \mathcal{N}$. .	24
3.19	RESIT & different noise levels & decoupled estimation & $Y = \mathcal{L}^3 + \mathcal{U}$. .	24
3.20	RESIT & different noise levels & coupled estimation & $Y = \mathcal{N} + \mathcal{N}$	28
3.21	RESIT & different noise levels & coupled estimation & $Y = \mathcal{N} + \mathcal{U}$	28
3.22	RESIT & different noise levels & coupled estimation & $Y = \mathcal{N} + \mathcal{L}$	29
3.23	RESIT & different noise levels & coupled estimation & $Y = \mathcal{N}^3 + \mathcal{N}$. . .	29
3.24	RESIT & different noise levels & coupled estimation & $Y = \mathcal{N}^3 + \mathcal{U}$. . .	30
3.25	RESIT & different noise levels & coupled estimation & $Y = \mathcal{N}^3 + \mathcal{L}$. . .	30
3.26	RESIT & different noise levels & coupled estimation & $Y = \mathcal{U} + \mathcal{U}$	31
3.27	RESIT & different noise levels & coupled estimation & $Y = \mathcal{U} + \mathcal{N}$	31
3.28	RESIT & different noise levels & coupled estimation & $Y = \mathcal{U} + \mathcal{L}$	32
3.29	RESIT & different noise levels & coupled estimation & $Y = \mathcal{U}^3 + \mathcal{U}$	32
3.30	RESIT & different noise levels & coupled estimation & $Y = \mathcal{U}^3 + \mathcal{N}$. . .	33
3.31	RESIT & different noise levels & coupled estimation & $Y = \mathcal{U}^3 + \mathcal{L}$	33
3.32	RESIT & different noise levels & coupled estimation & $Y = \mathcal{L} + \mathcal{L}$	34
3.33	RESIT & different noise levels & coupled estimation & $Y = \mathcal{L} + \mathcal{N}$	34
3.34	RESIT & different noise levels & coupled estimation & $Y = \mathcal{L} + \mathcal{U}$	35

3.35	RESIT & different noise levels & coupled estimation & $Y = \mathcal{L}^3 + \mathcal{L}$	35
3.36	RESIT & different noise levels & coupled estimation & $Y = \mathcal{L}^3 + \mathcal{N}$	36
3.37	RESIT & different noise levels & coupled estimation & $Y = \mathcal{L}^3 + \mathcal{U}$	36
3.38	$Y = X + N_y$. Contains all cases where X and N_y are drawn from the same type of distribution. Dashed lines are non-linear cases. Decoupled estimation (80% split).	41
3.39	$Y = X + N_y$. Contains all cases where $X \sim \mathcal{N}$ and $N_y \not\sim \mathcal{N}$. Dashed lines are non-linear cases. Decoupled estimation (80% split).	41
3.40	$Y = X + N_y$. Contains all cases where $X \sim \mathcal{U}$ and $N_y \not\sim \mathcal{U}$. Dashed lines are non-linear cases. Decoupled estimation (80% split).	42
3.41	$Y = X + N_y$. Contains all cases where $X \sim \mathcal{L}$ and $N_y \not\sim \mathcal{L}$. Dashed lines are non-linear cases. Decoupled estimation (80% split).	42
3.42	$Y = X + N_y$. Contains all cases where X and N_y are drawn from the same type of distribution. Dashed lines are non-linear cases. Coupled estimation.	43
3.43	$Y = X + N_y$. Contains all cases where $X \sim \mathcal{N}$ and $N_y \not\sim \mathcal{N}$. Dashed lines are non-linear cases. Coupled estimation.	43
3.44	$Y = X + N_y$. Contains all cases where $X \sim \mathcal{U}$ and $N_y \not\sim \mathcal{U}$. Dashed lines are non-linear cases. Coupled estimation.	44
3.45	$Y = X + N_y$. Contains all cases where $X \sim \mathcal{L}$ and $N_y \not\sim \mathcal{L}$. Dashed lines are non-linear cases. Coupled estimation.	44
3.46	Left: $X \sim \mathcal{N}, N_y \sim \mathcal{U}$. Right: $X \sim \mathcal{U}, N_y \sim \mathcal{L}$	48
3.47	Left: $X \sim \mathcal{U}^3, N_y \sim \mathcal{U}$. Right: $X \sim \mathcal{U}^3, N_y \sim \mathcal{N}$	48
4.1	$Y = X + N_y$. Contains all linear cases.	53
4.2	$Y = X^3 + N_y$. Contains all non-linear cases.	53

Chapter 1

Introduction

Due to the technological and computational advances during the last decades, scientist were able to tackle non-trivial problems from different research areas successfully. One of these research areas is causality. The fundamentals of causality is to determine causal relationship between two or more variables in a system. For example, given altitude and temperature we want to answer the question if temperature has an effect on altitude, or if altitude has an effect on temperature. This is of particular interest since if such a causal relationship is known then one can predict the effects on a system in case of intervention or perturbation. One method to determine causal relationships in a system is controlled experimentation (A/B tests) in which there are two identical groups with only one variation. The only variable that is varied (intervened on) is the potential cause. This procedure allows estimating causal effect of this variable in the given system. For example, testing the efficacy of medications is done within A/B tests. The control group receives no medication or a placebo, and the intervention group receives the real medication. The results often show the true effect (if any) of the medication on the human health. However, such tests are often too expensive, unethical or even technically impossible to execute. Therefore, it is of great interest to determine causal relationships from observational data only (e.g., structure learning).

1.1 State of the Art

Structure learning is the procedure to determine causal relationship directions from observational data only and representing these as a (causal) graph. The basic idea emerged from Wright (1921) as *path analysis*. This is used to describe directed dependencies among a set of variables and includes various models such as ANOVA, ANCOVA, etc. In his work, Wright made a distinction between three possible types of causal substructures which were allowed in a directed acyclic (no cycles) graph: 1) $X \rightarrow Y \rightarrow Z$, 2) $X \leftarrow Y \rightarrow Z$, and 3) $X \rightarrow Y \leftarrow Z$. Rebane and Pearl (2013) developed an algorithm to recover directed acyclic graphs from statistical data, which relied on this distinction of the previously 3 mentioned substructures. In general, one can easily identify the skeleton of a graph (that is the graph without arrows on the edges) and then partially identify the arrows (partially, because the three substructures' skeletons are identical but only 3) is distinguishable from others). Spirtes, Glymour, and Scheines (1993) and Spirtes et al. (2000) used Bayes networks to axiomatize the connection between causal structure and probabilistic independence and formalized under what assumptions one could draw causal knowledge from observational data only. Furthermore, they also formalized how incomplete causal knowledge could be used for causal intervention. Judea Pearl presented

in his work (Judea, 2000) a comprehensive theory of causality and unified the probabilistic, manipulative, counterfactual, and structural approaches to causation. Judea also introduced precise mathematical definitions of causal analysis for the standard curricula of statistics. From the work Judea (2000) we have the following key point: if there is a statistical association, e.g. two variables X, Y are dependent, then one of the following is true: 1) there is a causal relationship, either X has an effect on Y or Y has an effect on X ; 2) there is a common cause (confounder) that has effect on both X and Y ; 3) there is a possibly unobserved common effect of X and Y that is conditioned upon data acquisition (selection bias); or 4) there can be a combination of these. From there on a lot of research has been conducted to develop theoretical approaches and methods for identifying causal relationships from observational data only. Before we present some major works from the last two decades, we introduce the common concept behind all these approaches in a short formal manner.

In general, all these methods exploit the complexity of the marginal and conditional probability distributions in some way (e.g., Janzing et al. (2012) and Sgouritsa et al. (2015)) and under certain assumptions these methods are then able to solve the task of causal discovery. Let C denote the cause and E the effect. In a system with two or more variables we might have cause-effect pairs and then their joint density can be expressed with $p_{C,E}(c, e)$. This joint density can be factorized into either 1) $p_C(c) \cdot P_{E|C}(e|c)$ or 2) $p_E(e) \cdot P_{C|E}(c|e)$. The idea is then that 1 gives models of lower total complexity than 2 and this allows us to draw conclusions about the causal relationship direction. Intuitively this makes sense, because the effect contains information from the cause but not vice-versa (of course under the assumption that there are no cycles aka feedback loops). Therefore, 2 has at least as much complexity as 1. However, the definition of complexity is ambiguous. For example, one can say that " p_C contains no information about $P_{E|C}(e|c)$ " and then is able to draw partial conclusions about the causal direction of the given system. This complexity question is often colloquially referred to as "*breaking the symmetry*" (that is $p_C(c) \cdot P_{E|C}(e|c) \neq p_E(e) \cdot P_{C|E}(c|e)$).

Friedman and Nachman (2013) addressed the problem of learning the structure of a Bayesian network in domains which contain continuous variables. In their work they showed that in probabilistic networks with continuous variables one can use Gaussian Process priors to compute marginal likelihoods for structure learning.

Kano and Shimizu (2003) developed a model for causal inference using non-normality of observed data and improved path analysis (Wright, 1921) using non-normal data. Shimizu et al. (2006) proposed a method on how to determine the complete causal graph of continuous data under three assumptions: the data generating process is linear, no unobserved confounders, and noise variables have non-Gaussian distributions of non-zero variances. This method was not scale-invariant, but in a later work (Shimizu, Hyvarinen, and Kawahara, 2014) this problem had been addressed and a new method was proposed which was guaranteed to converge to the right solution within a small fixed number of steps if the data strictly followed the model.

Sun, Janzing, and Schölkopf (2006) introduced a method based on comparing the conditional distributions of variables given their direct causes for all hypothetical causal directions and choosing the most plausible one (Markov kernels). Those Markov kernels which maximize the conditional entropies constrained by their observed expectation, variance and covariance with its direct causes based on their given domain are considered as plausible kernels. Sun, Janzing, and Schölkopf (2008) continued the work on kernels by using the concept of reproducing kernel Hilbert spaces.

Hoyer et al. (2009) generalized the linear framework of additive noise models to nonlinear

models. Additive noise models are models in which the effect is a function of the cause and some random and non-observed additive noise term. For continuous variables, earlier methods often assumed linear models for the independence tests. However, if data contained non-Gaussian variables, then this can help in distinguishing the causal directions and identify the causal graph.

Janzing, Hoyer, and Schölkopf (2009) proposed a method for inferring linear causal relationships among multi-dimensional variables by factorizing the joint distribution into products with marginal and conditional distributions (as seen above with 1 and 2). Then, in one of these products the factors (e.g., $P(E)$ and $P(C|E)$) satisfy non-generic relations indicating that $E \rightarrow C$ is wrong.

Mooij et al. (2009) introduced a method which minimizes the statistical dependence between the regressors and residuals. If residuals (the difference between actual output and predicted output) are no longer dependent on the input, then regression can successfully model the dependence of the output on the input. This method does not need to assume a particular distribution of the noise because any form of regression can be used (e.g., Linear Regression) and is well suited for the task of causal inference in additive noise models.

Stegle et al. (2010) created a method to model observed data by using probabilistic latent (hidden) variable models, which incorporate the effects of unobserved noise. To analyze the joint density of cause and effect, the effect is modeled as a function of the cause and some independent noise (not necessarily additive). With general non-parametric priors on this function and on the distribution of the cause the causal direction is then determined by using standard Bayesian model selection.

Mooij et al. (2011) introduced a method to determine causal relationship in cyclic additive noise models and state that such models are generally identifiable in the bivariate, Gaussian-noise case. Their method works for continuous data and can be seen as a special case of nonlinear independent component analysis.

Zhang and Hyvarinen (2012) tested the stability of the identifiability of post-nonlinear models with two variables and listed all cases in which this model is not identifiable anymore. Furthermore, they showed how to approach multivariate cases with post-nonlinear models.

Daniusis et al. (2012) showed that even in deterministic cases (noise-free cases) there are asymmetries that can be exploited for causal inference. Their method is based on the idea that if $X \rightarrow Y$ then the distribution of X and the function mapping X to Y must be independent since they correspond to independent mechanisms of nature.

Hyvärinen and Smith (2013) proposed a method which is based on the likelihood ratio under the linear non-Gaussian acyclic model (LiNGAM, Shimizu (2014)) and therefore not resorting to independent component analysis algorithm as previous methods did.

Peters and Bühlmann (2013) proved full identifiability of linear Gaussian structural equation models if all the noise variables have the same variance (*full identifiability* means that not only the skeleton of the causal graph is recoverable but also the arrows).

Peters et al. (2014) proposed a method that can identify the directed acyclic graph from the distribution under mild conditions. In contrast, other methods assumed faithfulness and could only identify the Markov equivalence class of the graph (*Markov equivalence class* refers to the class of graphs where all graphs have the same skeletons).

Nowzohour and Bühlmann (2016) proposed to use penalized likelihood scores instead of independence scores to determine the true causal graph from the Markov equivalence class.

Park and Kim (2019) and Chen, Drton, and Wang (2019) proved that linear Gaussian models where noise variables have different error variance can be identifiable by ordering

variables according to the law of total variances and then performing independence tests between variables.

Despite all the research in the past years one small but nonetheless important aspect of causal discovery methods has not received much attention: can different noise levels have an impact on the correctness of these methods. In real world, observational data often differs in terms of noise level. Usually, these levels do not differ significantly but it can occur that noise levels change drastically from cause to effect. For example, if the data collection process has a lot of interference (e.g., in outer space) then such noise levels can differ a lot.

In this work we will focus on the *Additive Noise Models* (ANMs) as they are well established and yielded many good results (Kpotufe et al. (2014)). ANMs are heavily based on the presence of noise and thus our research question is then formulated as follows: *how do different noise levels of the additive noise impact the correctness of ANM methods?* For this work, two specific methods have been selected to test this question: *Regression with Subsequent Independence Test (RESIT)* (Peters et al., 2014) and *Identification using Conditional Variances (Uncertainty Scoring)* (Park, 2020). Both methods yielded good results and can be used even when variables have different distribution types (e.g., Laplace). The next chapter introduces Additive Noise Models in a formal manner, followed by standard notation definition. Chapters 3 and 4 contain the theory and experiments of the first and the second methods respectively. The last chapter draws conclusions and discusses possible future work.

Chapter 2

Additive Noise Models and Notation

The two selected methods for this work can be used for additive noise models, although the second method is not limited to it (Park and Kim (2019)). In general, such causal discovery methods exploit the additivity of the noise in order to determine the causal relationship between two or more variables. We will give now a short definition of additive noise models for the bivariate case only. For more details and for multivariate cases please refer to Hoyer et al. (2009) and Peters et al. (2014).

Let $X, Y \in \mathbb{R}$ be the cause and effect, respectively. Let there be also m latent (hidden) causes $U = (U_1, \dots, U_m) \in \mathbb{R}^m$. Then the causal relationship can be modeled as

$$\begin{cases} Y = f(X, U_1, \dots, U_m) \\ X \perp\!\!\!\perp U, X \sim p_X(x), U \sim p_U(u_1, \dots, u_m) \end{cases}$$

where $f : \mathbb{R} \times \mathbb{R}^m \rightarrow \mathbb{R}$ is a linear or nonlinear function, and $p_X(x)$ and $p_U(u_1, \dots, u_m)$ are the joint densities of the observed cause X and the latent causes U . We are assuming that there is no confounding, no selection bias, and no feedback loop between X and Y and therefore X and U are independent, which is denoted as $X \perp\!\!\!\perp U$. Since the latent causes U are unobserved, their influence can be summarized by a single noise variable $N_y \in \mathbb{R}$, and the model can be defined as follows:

$$\begin{cases} Y = f(X, N_y) \\ X \perp\!\!\!\perp N_y, X \sim p_X(x), N_y \sim p_{N_y}(n_y). \end{cases}$$

Notations

In the experiments, we are considering both linear and nonlinear additive noise models:

$$Y = \beta X + N_y \text{ with } \beta \in \mathbb{R}, \text{ for the linear case}$$

and

$$Y = \beta X^\alpha + N_y \text{ with } \beta, \alpha \in \mathbb{R}, \text{ for the nonlinear case.}$$

The arrow in " $X \rightarrow Y$ " signifies X has an effect on Y , or in other words, X is a cause of Y . X and N_y can be drawn from one of the following distributions: the normal distribution denoted by the calligraphic letter \mathcal{N} , the uniform distribution denoted by the calligraphic letter \mathcal{U} , or the laplace distribution denoted by the calligraphic letter \mathcal{L} . For example, throughout this work " X is drawn from a normal distribution" is denoted as $X \sim \mathcal{N}$ or $X \sim \mathcal{N}(\mu_x, \sigma_x^2)$ with μ_x standing for the mean and σ_x^2 for the variance. The

Structural causal model of a directed acyclic graph (DAG) refers to the equations of the cause and effects. For example, the equation $Y = f(X, N_y)$ refers to the DAG in Fig. 2.1 and also composes the entire structural equation model of that DAG (since there are no other variables in that DAG). In Fig. 2.2 the structural equation model looks as follows:

$$\begin{cases} A = f(Y, N_a) \\ B = f(A, N_b) \\ X = f(B, N_x) \end{cases}$$

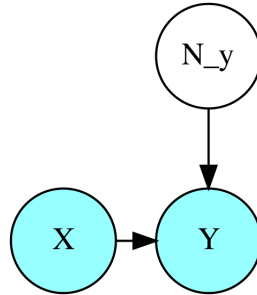


Figure 2.1: A simple directed acyclic graph showing causal relationships between variables.

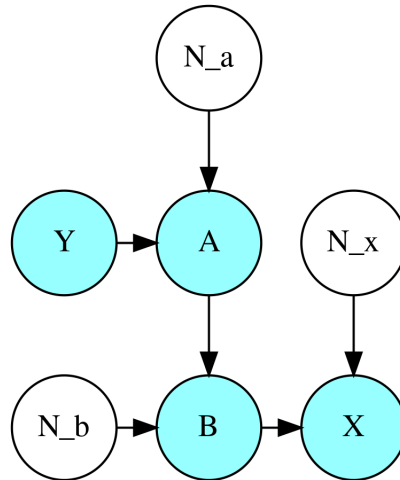


Figure 2.2: Another directed acyclic graph showing causal relationships between variables.

As we are only considering bivariate cases, we only have one equation and therefore *structural equation model*, *structural equation* and *equation* are used interchangeably. Lastly, we introduce the four following terms (with abbreviations): parent (Pa), antecedent (An), descendent (De) and non-descendent (Nd). These notations are used to describe the relationship between two variables in a causal graph. Parent is the direct antecedent of a node (e.g., $Pa(A) = Y$ in Fig. 2.2). A descendent of a (starting) variable is any variable which can be reached from the starting variable following a directed path (e.g., $De(Y) = \{A, B, X\}$ in Fig. 2.2). Non-descendent is the opposite, i.e. cannot be reached following a directed path (e.g., $Nd(Y) = \{N_a, N_b, N_x\}$). Finally, the antecedent is any starting variable for a descendent (e.g., $An(X) = \{Y, A, B, N_x, N_a, N_b\}$).

2.1 Experiment Layout

One additional part of the experiments is to see whether splitting data into training and test data is beneficial or not. However, as some experiments did not allow us to split data and/or the results were too small to be contained in an own subsection it is not quite obvious from the contents table where data splitting occurred or not. The following Table 2.1 thus shall provide an overview where we applied splitting data and where not. Furthermore, throughout this work splitting data is referred to as *decoupled estimation* and not splitting data is referred to as *coupled estimation*, both terms originate from Kpotufe et al. (2014).

Section	Type	Decoupled	Coupled
Section 3.1	RESIT & different noise levels	✓	
Section 3.2	RESIT & different noise levels		✓
Section 3.3	RESIT & different noise levels & no prior assumption	✓	✓
Section 3.4	RESIT & different means	✓	
Chapter 4	Uncertainty Scoring		✓

Table 2.1: Experiments Layout for Decoupled and Coupled estimation.

We have uploaded all source codes and results on a Gitlab repository: <https://gitlab.com/Shinkaiika/noise-level-causal-identification-additive-noise-models/>

Chapter 3

Experiments on Regression with Subsequent Independence Test

This chapter is an empirical study which involves testing the performance of *Regression with Subsequent Independence Test (RESIT)* methods (Peters et al., 2014) for additive noise models (ANM) (Hoyer et al., 2009; Kpotufe et al., 2014; Mooij et al., 2016) given i.i.d data from a joint distribution to try to estimate the corresponding directed acyclic graph (DAG). This chapter is divided into four sections. The first three sections (Section 3.1 to Section 3.3) contain the main work of this chapter. In Section 3.1 we test RESIT with different noise levels and decoupled estimation. In Section 3.2 we test RESIT with different noise levels and coupled estimation. In Section 3.3 we test RESIT with different noise levels and both decoupled and coupled estimation, but without the prior assumption (which says that exactly one causal direction must be present in the bi-variate case). In Section 3.4 we perform tests on RESIT with different means (for both the cause variable and the noise term). For all experiments we generate artificial data using linear and non-linear functions. While both linear and non-linear data can be identifiable in causal models, non-linearity helps in identifying the causal direction as was shown by Hoyer et al. (2009). Therefore, we consider both cases in our experiments in order to investigate how different noise levels affect causal discovery for linear and on non-linear data. In all experiments we use the equation $Y = X + N_Y$ for the linear cases and $Y = X^3 + N_Y$ for the non-linear cases. These two structural causal models have been selected arbitrarily for simplicity. For the consistency of the identifiability of linear and non-linear data in additive noise models, the reader is referred to Shimizu et al. (2006), Hoyer et al. (2009), Zhang and Hyvarinen (2012), and Kpotufe et al. (2014). Finally, in both sections we will also measure performance difference when deploying decoupled estimation (splitting data into training and test data) and coupled estimation (no splitting), see Kpotufe et al. (2014), Mooij et al. (2016).

3.1 RESIT with Different Noise Levels

The first section of experiments involves testing different noise levels for the additive noise term and to see whether it has an impact on the accuracy of RESIT methods or not. The RESIT method is based on the fact that for each node X_i the corresponding noise variable N_i is independent of all non-descendants of X_i . For example, in a DAG, if we have $Y = X_1 + N_1$ then $X_1 \perp\!\!\!\perp N_1$. Following this idea we visit every single node in a specific order. To determine this order we do an iterative process where in each step we determine the next node in the order. To determine the next node we look for a *sink* node.

This is done by regressing each single variable on all other variables and then measuring the independence between the residuals and those other variables, and finally selecting the single variable which led to the least dependent residuals. After this iterative process, the order is established and every node is visited again. We then eliminate incoming edges until the residuals are not independent anymore. We will restrict our experiments to bivariate cases only to reduce runtimes. The authors in Peters et al. (2014) generalized RESIT to multivariate cases and proved identifiability. In our experiments we then have two variables, X and Y , and the task is to determine whether X causes Y ($X \rightarrow Y$) or Y causes X ($Y \rightarrow X$).

3.1.1 Setup

For all empirical tests we assume X to be a cause of Y , that is $X \rightarrow Y$. In the sense of additive noise models, the equation is then:

$$Y = \beta X + N_y$$

$$(Y = \beta X^3 + N_y \text{ for the non-linear case})$$

where

$$\beta = 1,$$

and

$$X \sim \begin{cases} \mathcal{N}(0, 1) & \text{or} \\ \mathcal{U}(-1, 1) & \text{or} \\ \mathcal{L}(0, 1) \end{cases}$$

and

$$N_y \sim \begin{cases} \mathcal{N}(0, 1 \cdot i) & \text{or} \\ \mathcal{U}(-1 \cdot i, 1 \cdot i) & \text{or} \\ \mathcal{L}(0, 1 \cdot i) \end{cases}$$

with i being a scaling factor for the noise level in N_y . The goal is to analyze how different standard deviations (boundaries for the uniform case) in the noise term N_y relative to the standard deviation (or boundaries for the uniform case) in the X term impact the RESIT method.

We apply the same algorithm as Algorithm 1 in Mooij et al. (2016) which requires inputs X and Y , a regression method and a score estimator $\hat{C} : \mathbb{R}^N \times \mathbb{R}^N \rightarrow \mathbb{R}$ and outputs *dir* (casual relationship **direction**). First, the data is split into training data (80%) and test data (20%). Kpotufe et al. (2014) refers to this as "decoupled estimation". The training data is used to fit the regression model and the test data is used for the estimator. The idea is to regress Y on X with the training data, predict \hat{Y} with the test data and then calculate residuals $Y_{res} = \hat{Y} - Y_{Test}$. Y_{res} and X_{Test} are then used in the criterion step, where we use several estimators independently and receive $\hat{C}_{X \rightarrow Y}$, a score for the assumed case $X \rightarrow Y$. Similarly, to test the other case ($Y \rightarrow X$), we regress X on Y , calculate residuals $X_{res} = \hat{X} - X_{Test}$ and estimate $\hat{C}_{Y \rightarrow X}$. In our test scenario our generated data always follows $X \rightarrow Y$. This verifies the **assumption** that only one direction in our data is correct (and not both) and therefore we can compare both scores directly in order to make a decision on the cause-effect direction. Thus, for independence tests, we can compare estimates directly and we do not need to determine the value of α

for the independence tests. Algorithm 1 shows pseudo code of the procedure explained above.

Algorithm 1 General procedure to decide whether $p(x, y)$ satisfies Additive Noise Model $X \rightarrow Y$ or $Y \rightarrow X$ with decoupled estimation.

```

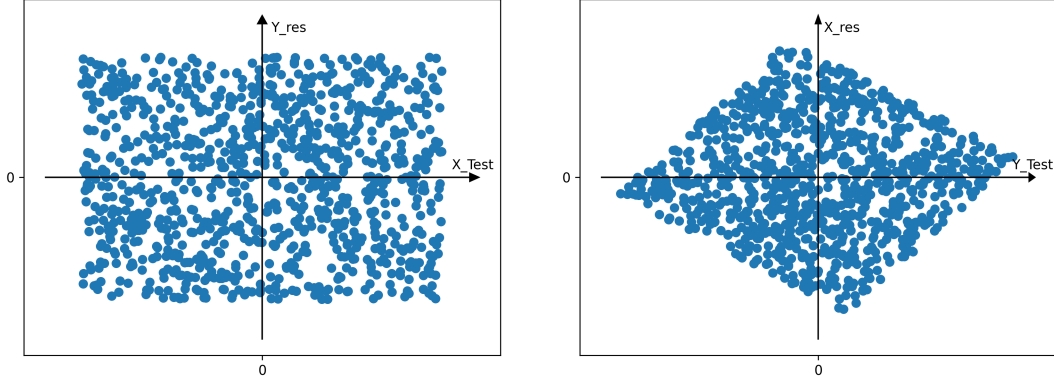
1: Input:
2:   1) I.i.d. sample data  $X$  and  $Y$ 
3:   2) Regression method
4:   3) Score estimator  $\hat{C} : \mathbb{R}^N \times \mathbb{R}^N \rightarrow \mathbb{R}$ 
5: Output:
6:    $dir$ 
7:
8: Procedure
9: 1) Split data into training and test data:
10:  $X_{Train}, X_{Test} \leftarrow X$ 
11:  $Y_{Train}, Y_{Test} \leftarrow Y$ 
12:
13: 2) Train regression models
14:  $reg_1 \leftarrow$  Regress  $Y_{Train}$  on  $X_{Train}$ 
15:  $reg_2 \leftarrow$  Regress  $X_{Train}$  on  $Y_{Train}$ 
16:
17: 3) Calculate Residuals:
18:  $Y_{res} = reg_1.predict(X_{Test}) - Y_{Test}$ 
19:  $X_{res} = reg_2.predict(Y_{Test}) - X_{Test}$ 
20:
21: 4) Calculate Scores:
22:  $\hat{C}_{X \rightarrow Y} = \hat{C}(X_{Test}, Y_{res})$ 
23:  $\hat{C}_{Y \rightarrow X} = \hat{C}(Y_{Test}, X_{res})$ 
24:
25: 5) Finally, output direction  $dir$ :

```

$$dir = \begin{cases} X \rightarrow Y & \text{if } \hat{C}_{X \rightarrow Y} < \hat{C}_{Y \rightarrow X}, \\ Y \rightarrow X & \text{if } \hat{C}_{X \rightarrow Y} > \hat{C}_{Y \rightarrow X}, \\ ? & \text{if } \hat{C}_{X \rightarrow Y} = \hat{C}_{Y \rightarrow X}. \end{cases} \quad (3.1)$$

Fig. 3.1 explains the concept graphically. The left-hand side of the figure shows a scatter plot of X_{Test} and Y_{res} . As one can see, given any input for X_{Test} the range does not change, and therefore X_{Test} and Y_{res} are independent. The right-hand side of the figure shows the opposite case. For any given input, the range does change. This means that Y_{Test} and X_{res} are dependent and Y_{Test} contains some information of X_{res} (which contradicts our assumption of independent noise!). This allows us to draw conclusions about the causal relationship direction and therefore we know that X is the cause and not vice-versa. This illustrates the estimation step Eq. (3.1) in Algorithm 1.

For the regression, Linear Regression is used. Linear regression can also be used in the non-linear case when an appropriate coordinates transformation is applied. For the estimator several different scores can be used. In our experiments we used six different independence tests and six different entropy measures for the estimation criterion. In



(a) Regress Y on X .

(b) Regress X on Y .

Figure 3.1: Data is generated following $Y = X + N_y$ with uniform distributions only.

general, for the independence tests we have:

$$\hat{C}(X_{Test}, Y_{res}) = I(X_{Test}, Y_{res})$$

with $I(\cdot, \cdot)$ being any independence test.

In the case of entropy estimators we have:

$$\hat{C}(X_{Test}, Y_{res}) = H(X_{Test}) + H(Y_{res}),$$

with $H(\cdot)$ being any entropy measure. The estimator score for entropy is derived from Lemma 1 in Kpotufe et al. (2014):

Lemma 1 Consider a joint distribution of X, Y with density $p(x, y)$. For arbitrary functions $f, g: \mathbb{R} \rightarrow \mathbb{R}$ we have:

$$H(X) + H(Y - f(X)) = H(Y) + H(X - g(Y)) - I(X - g(Y), Y) + I(Y - f(X), X), \quad (3.2)$$

where $H(\cdot)$ denotes differential Shannon entropy, and $I(\cdot, \cdot)$ denotes differential mutual information (Cover (1999)).

The above Lemma can be proven with the chain rule of differential entropy (see Kpotufe et al. (2014)). If the density $p(x, y)$ satisfies an identifiable ANM $X \rightarrow Y$, then there exists a function f with $I(Y - f(X), X) = 0$ (e.g., the regression function $x \mapsto \mathbb{E}(Y|X = x)$), but $I(X - g(Y), Y) > 0$ for any function g . Therefore, in the case of $X \rightarrow Y$, in 3.2 we have:

$$H(X) + H(Y - f(X)) < H(Y) + H(X - g(Y))$$

which is equivalent to the first row in 3.1:

$$\hat{C}_{X \rightarrow Y} < \hat{C}_{Y \rightarrow X}.$$

The following estimators were used in this work. The implementation of estimators with numbers 2 - 12 was taken from the *information theoretical estimators* toolbox Szabó (2014):¹

1. **HSIC**: Hilbert-Schmidt Independence Criterion with RBF Kernel ²

$$I_{HSIC}(x, y) := \|C_{xy}\|_{HS}^2$$

where C_{xy} is the cross-covariance operator and HS the squared Hilbert-Schmidt norm.

2. **HSIC_IC**: Hilbert-Schmidt Independence Criterion using incomplete Cholesky decomposition (low rank decomposition of the Gram matrices, which permits an accurate approximation to HSIC as long as the kernel has a fast decaying spectrum) which has $\eta = 1 * 10^{-6}$ precision in the incomplete cholesky decomposition.
3. **HSIC_IC2**: Same as HSIC_IC but with $\eta = 1 * 10^{-2}$.
4. **DISTCOV**: Distance covariance estimator using pairwise distances. This is simply the L_w^2 norm of the characteristic functions φ_{12} and $\varphi_1\varphi_2$ of input x, y :

$$\varphi_{12}(\mathbf{u}^1, \mathbf{u}^2) = \mathbb{E}[e^{i\langle \mathbf{u}^1, \mathbf{x} \rangle + i\langle \mathbf{u}^2, \mathbf{y} \rangle}],$$

$$\varphi_1(\mathbf{u}^1) = \mathbb{E}[e^{i\langle \mathbf{u}^1, \mathbf{x} \rangle}],$$

$$\varphi_2(\mathbf{u}^2) = \mathbb{E}[e^{i\langle \mathbf{u}^2, \mathbf{y} \rangle}].$$

With $i = \sqrt{-1}$, $\langle \cdot, \cdot \rangle$ the standard Euclidean inner product and \mathbb{E} the expectation. Finally, we have:

$$I_{dCov}(x, y) = \|\varphi_{12} - \varphi_1\varphi_2\|_{L_w^2}$$

5. **DISTCORR**: Distance correlation estimator using pairwise distances. It is simply the standardized version of the distance covariance:

$$I_{dCor}(x, y) = \begin{cases} \frac{I_{dCov}(x, y)}{\sqrt{I_{dVar}(x, x)I_{dVar}(y, y)}}, & \text{if } I_{dVar}(x, x)I_{dVar}(y, y) > 0 \\ 0, & \text{otherwise,} \end{cases}$$

with

$$I_{dVar}(x, x) = \|\varphi_{11} - \varphi_1\varphi_1\|_{L_w^2}, \quad I_{dVar}(y, y) = \|\varphi_{22} - \varphi_2\varphi_2\|_{L_w^2}$$

(see characteristic functions under 3. DISTCOV)

6. **HOEFFDING**: Hoeffding's Phi

$$I_{\Phi}(x, y) = I_{\Phi}(C) = \left(h_2(d) \int_{[0,1]^d} [C(\mathbf{u}) - \Pi(\mathbf{u})]^2 d\mathbf{u} \right)^{\frac{1}{2}}$$

with C standing for the copula of the input and Π standing for the product copula.

¹More details on the estimators is given in the documentation of the toolbox.

²Source: <https://github.com/amber0309/HSIC>

7. **SH_KNN**: Shannon differential entropy estimator using kNNs (k-nearest neighbors)

$$H(\mathbf{Y}_{1:T}) = \log(T-1) - \psi(k) + \log(V_d) + \frac{d}{T} \sum_{t=1}^T \log(\rho_k(t))$$

with T standing for the number of samples, $\rho_k(t)$ - the Euclidean distance of the k^{th} nearest neighbour of \mathbf{y}_t in the sample $\mathbf{Y}_{1:T} \setminus \{\mathbf{y}_t\}$ and $V \subseteq \mathbb{R}^d$ a finite set.

8. **SH_KNN_2**: Shannon differential entropy estimator using kNNs with $k=3$ and kd-tree for quick nearest-neighbour lookup
9. **SH_KNN_3**: Shannon differential entropy estimator using kNNs with $k=5$
10. **SH_MAXENT1**: Maximum entropy distribution-based Shannon entropy estimator

$$H(\mathbf{Y}_{1:T}) = H(n) - \left[k_1 \left(\frac{1}{T} \sum_{t=1}^T G_1(y'_t) \right)^2 + k_2 \left(\frac{1}{T} \sum_{t=1}^T G_2(y'_t) - \sqrt{\frac{2}{\pi}} \right)^2 \right] + \log(\hat{\sigma}),$$

with

$$\hat{\sigma} = \hat{\sigma}(\mathbf{Y}_{1:T}) = \sqrt{\frac{1}{T-1} \sum_{t=1}^T (y_t)^2},$$

$$y'_t = \frac{y_t}{\hat{\sigma}}, (t = 1, \dots, T)$$

$$G_1(z) = z e^{-\frac{z^2}{2}},$$

$$G_2(z) = |z|,$$

$$k_1 = \frac{36}{8\sqrt{3} - 9},$$

$$k_2 = \frac{1}{2 - \frac{6}{\pi}},$$

11. **SH_MAXENT2**: Maximum entropy distribution-based Shannon entropy estimator, same as SH_MAXENT1 with the following changes:

$$G_2(z) = e^{-\frac{z^2}{2}},$$

$$k_2 = \frac{24}{16\sqrt{3} - 27},$$

12. **SH_SPACING_V**: Shannon entropy estimator using Vasicek's spacing method.

$$H(\mathbf{Y}_{1:T}) = \frac{1}{T} \sum_{t=1}^T \log \left(\frac{T}{2m} [y_{(t+m)} - y_{(t-m)}] \right)$$

with T number of samples, the convention that $y_{(t)} := y_{(1)}$ if $t < 1$ and $y_{(t)} := y_{(T)}$ if $t > T$ and $m = \lfloor \sqrt{T} \rfloor$.

3.1.2 Execution

First, 199 different i factors have been generated:

$$i \in \{0.01, 0.02, \dots, 1.00\} \cup \{1, 2, \dots, 100\}$$

For each i every linear and non-linear combination of distribution types have been tested (18 in total). That is, we have the general structures $Y = X + N_y$ and $Y = X^3 + N_y$ where X and N_y are drawn from the three different distributions, \mathcal{N} , \mathcal{U} or \mathcal{L} .

$$Y = X \sim \mathcal{N} + N_y \sim \mathcal{N},$$

$$Y = X \sim \mathcal{N} + N_y \sim \mathcal{U},$$

$$\vdots$$

$$Y = X \sim \mathcal{L}^3 + N_y \sim \mathcal{U}.$$

Note that \mathcal{L}^3 here signifies the non-linear case $Y = X^3 + N_y$.

Next, for each of the 18 combinations we perform 100 tests each time. For every test we generate 1000 new samples for the distribution of X and the distribution of N_y .

Lastly, we simply count how many tests are successful in these 100 tests and define this ratio as our accuracy measure.

3.1.3 Experimental Results

In the following figures the y-axis shows the accuracy ($\frac{\#\text{successful tests}}{100}$) and the x-axis shows the range of the i factor. Each figure contains two subfigures, the left with $i \in \{0.01, 0.02, \dots, 1.00\}$ and the right figure with $i \in \{1, 2, \dots, 100\}$. If the values of the estimators shown in the plots are close to 0.5, then this means that in 50% of the tests the algorithm decided the correct direction (and vice versa 50% the wrong direction) and thus indicates **unidentifiability**. If plots are closer to accuracy 1 then we have very good/consistent **identifiability**. The legend for both subfigures is placed on the right side of the right subfigure and for the decoupled experiments the estimator names are suffixed with "_S", S(plit). However, in the analysis text the suffix is dropped for better readability. The next subsection describes each figure individually and the following subsection thereafter provides a summary and draws conclusions. Note that the first group of results are obtained with the assumption " $X \rightarrow Y \oplus Y \rightarrow X$ " and using decoupled estimation. Also the plots for DISTCOV (dark green) and DISTCORR (medium purple) often overlap (more than in 90% of cases), resulting in a dark purple line.

Individual Analysis

This section can be skipped as we provide a summary table in the next section (Table 3.1).

Fig. 3.2 shows the only case where we never achieve identifiability. This is the well known linear Gaussian structural causal model and has only recently been tackled successfully in Chen, Drton, and Wang (2019) and Park and Kim (2019).

Fig. 3.3 shows the linear model with $Y = \mathcal{N} + \mathcal{U}$, that is independent variable X being distributed according to the normal distribution and noise - according to uniform distribution. SH_SPACING_V performs the best with the accuracy of 100% for $i \in [0.55; 7]$. HSIC_IC and HSIC_IC2 perform the worst here with only an accuracy above 90% for $i \in [3; 7]$. All other estimators perform mediocre with an accuracy $> 80\%$ for $i \in [0.5; 7]$.

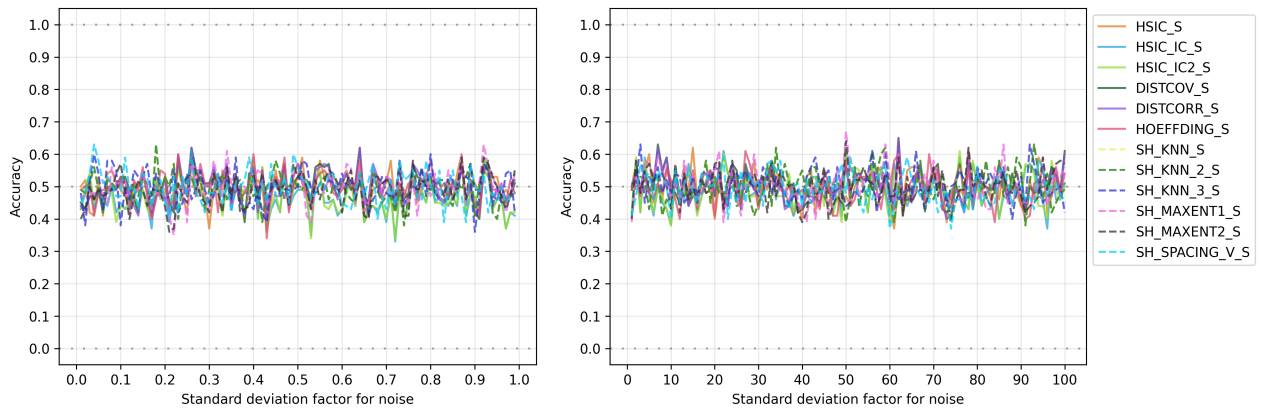


Figure 3.2: RESIT & different noise levels & decoupled estimation & $Y = \mathcal{N} + \mathcal{N}$

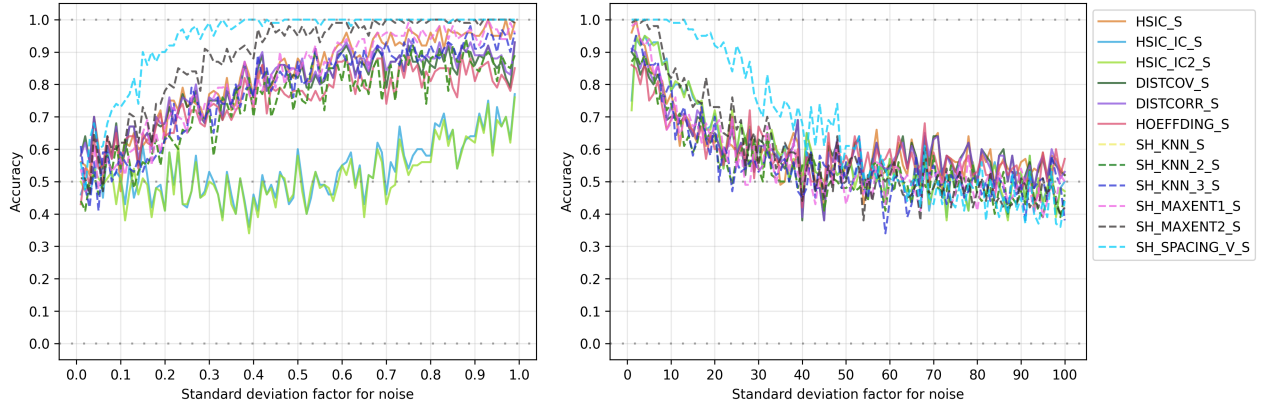


Figure 3.3: RESIT & different noise levels & decoupled estimation & $Y = \mathcal{N} + \mathcal{U}$

Fig. 3.4 shows the linear model $Y = \mathcal{N} + \mathcal{L}$. The best estimators are SH_MAXENT1 and SH_MAXENT2 with accuracy above 90% for $i \in [0.35; 2]$. HSIC also performs good with accuracy over 90% for $i \in [0.38; 2]$. The worst estimators are the three Shannon differential entropy estimators using kNNs which never remain consistently above 80% accuracy. The remaining estimators lie within the range $90\% \pm 8\%$ accuracy with $i \in [0.3; 3]$. Fig. 3.5 shows the non-linear model $Y = \mathcal{N}^3 + \mathcal{N}$. Here all estimators perform very good with $i \in [0.4; 25]$ having an accuracy of almost 100%. With $i < 0.3$ most estimators drop fast below 90% accuracy. With $i \in [20; 100]$ all estimators remain above 90% accuracy, except for HSIC_IC, HSIC_IC2, SH_MAXENT1 and SH_MAXENT2 which drop below 90% after $i = 45$. DISTCOV, SH_SPACING_V and the three Shannon kNN estimators remain close to 100% in $i \in [0.01; 100]$.

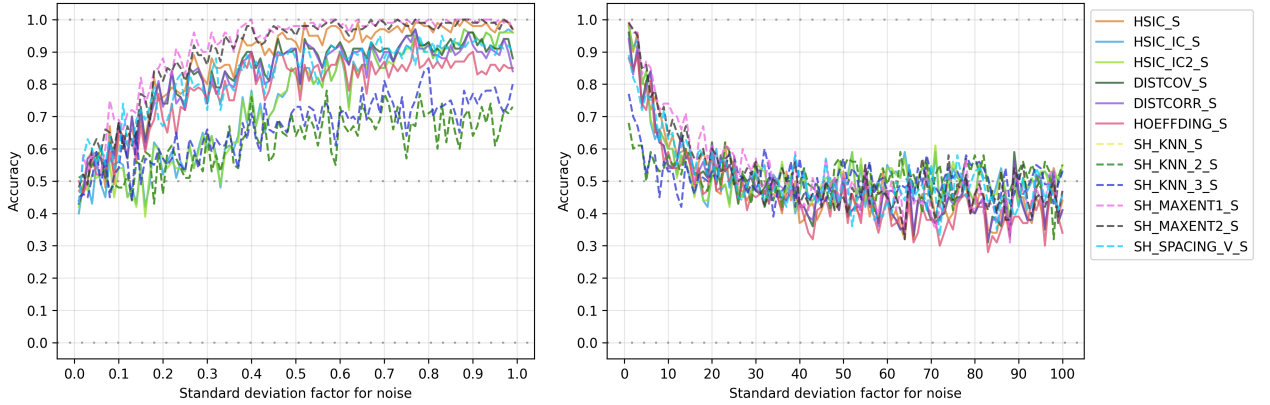


Figure 3.4: RESIT & different noise levels & decoupled estimation & $Y = \mathcal{N} + \mathcal{L}$

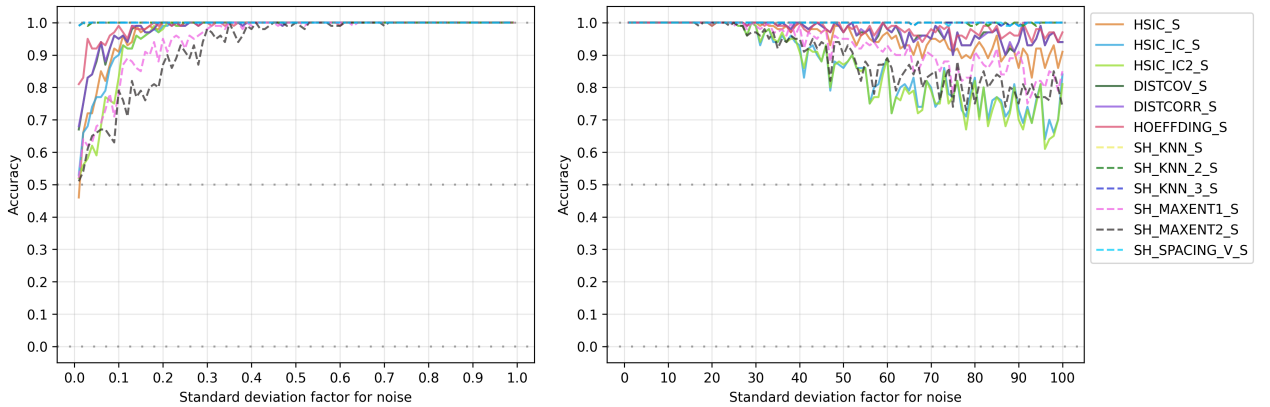


Figure 3.5: RESIT & different noise levels & decoupled estimation & $Y = \mathcal{N}^3 + \mathcal{N}$

Fig. 3.6 shows the non-linear model $Y = \mathcal{N}^3 + \mathcal{U}$. This result is similar as the previous one. With $i \in [0.45; 80]$ we have 90% or higher accuracy for all estimators. `DISTCOV`, `SH_SPACING_V` and the three Shannon kNN estimators remain close to 100% in $i \in [0.01; 100]$. Fig. 3.7 shows the non-linear model $Y = \mathcal{N}^3 + \mathcal{L}$. Here all estimators perform very good with $i \in [0.4; 30]$ having an accuracy close to 100%. With $i < 0.25$ all estimator drop rapidly and with $i > 30$ `HSIC_IC`, `HSIC_IC2`, `SH_MAXENT1` and `SH_MAXENT2` drop below 90% accuracy for higher i . All others remain over 90% accuracy while `HSIC` remains around 90%.

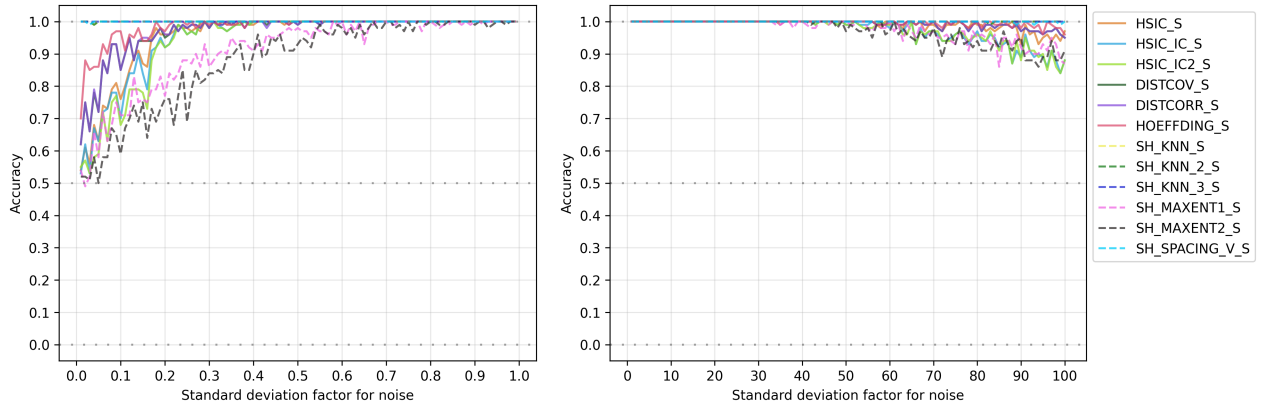


Figure 3.6: RESIT & different noise levels & decoupled estimation & $Y = \mathcal{N}^3 + \mathcal{U}$

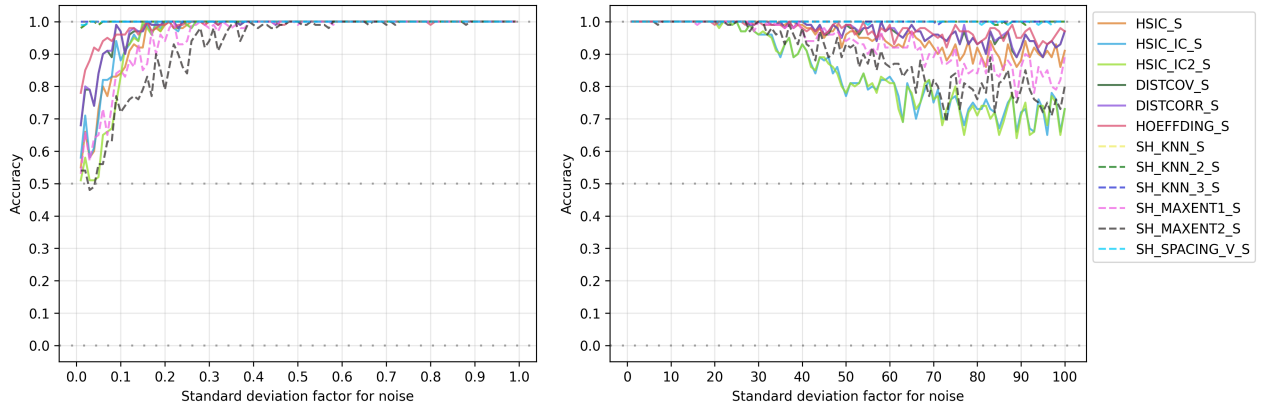


Figure 3.7: RESIT & different noise levels & decoupled estimation & $Y = \mathcal{N}^3 + \mathcal{L}$

Fig. 3.8 shows the linear model $Y = \mathcal{U} + \mathcal{U}$. HSIC_IC and HSIC_IC2 only reach accuracy above 90% around $i = 3$. All other estimator perform quite good with $i \in [0.3; 5]$ while only Hoeffding and DISTCOV drop slightly below 90% accuracy for $i = 1$. SH_SPACING_V has 100% accuracy for $i \in [0.12; 10]$ and has on the remaining i factors better accuracy than all other estimators. Fig. 3.9 shows the linear model $Y = \mathcal{U} + \mathcal{N}$. Here all estimators differ stronger than in the previous experiments. First, SH_SPACING_V is performing the best with 100% accuracy for $i \in [0.08; 2]$. With $i = 1$ all other estimators remain above 90%, expect Hoeffding ($\sim 88\%$) and HSIC_IC and HSIC_IC2 (both $\sim 75\%$). After $i = 2$ all estimators drop drastically towards 50% accuracy except SH_SPACING_V which remains above 70%. For $i \in [0.2; 1]$ some estimators remain between 80% and 95% while HSIC is above 95%. Only HSIC_IC and HSIC_IC2 perform worse than all other estimators.

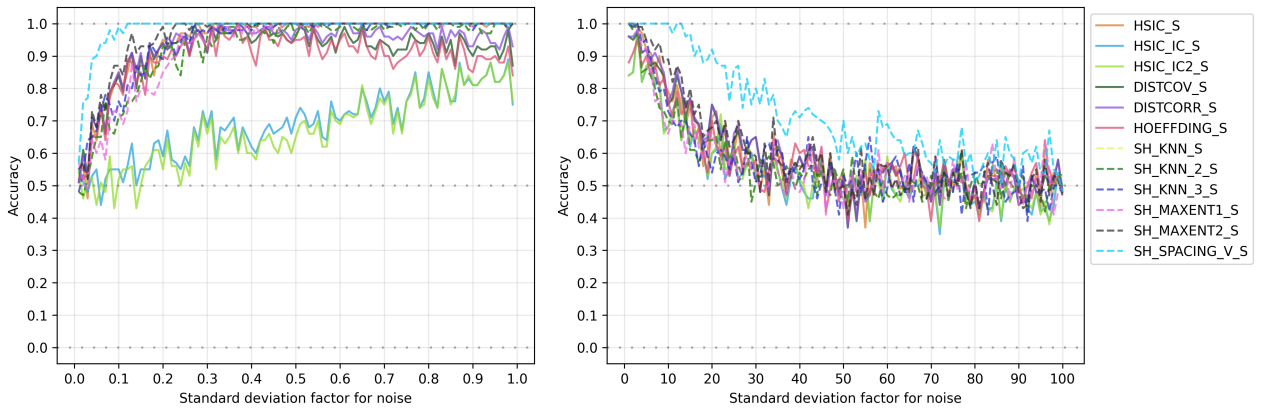


Figure 3.8: RESIT & different noise levels & decoupled estimation & $Y = \mathcal{U} + \mathcal{U}$

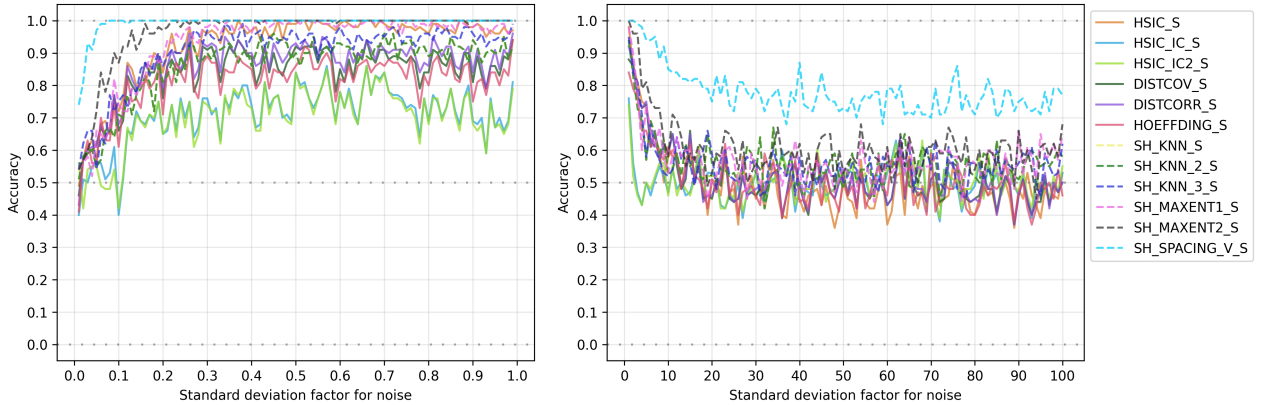


Figure 3.9: RESIT & different noise levels & decoupled estimation & $Y = \mathcal{U} + \mathcal{N}$

Fig. 3.10 shows the linear model $Y = \mathcal{U} + \mathcal{L}$. For $i \in [0.3; 1]$ all estimators perform well with 90% or higher accuracy, except HSIC_IC and HSIC_IC2 which remain above 90% accuracy only after $i = 0.45$. After $i = 1$ each estimator drops drastically and all converge towards 50% accuracy, except for SH_SPACING_V which remains with a mean of 70% accuracy higher than other estimators. For $i \in [0.08; 1]$ SH_SPACING_V also has accuracy 100%. For $i < 0.3$ all other estimators drop fast towards 50%. Fig. 3.11 shows the non-linear model $Y = \mathcal{U}^3 + \mathcal{U}$. For $i \in [0.09; 1]$ all estimators (except HSIC_IC and HSIC_IC2) remain above 95% accuracy, while SH_KNN, SH_KNN_2, and SH_SPACING_V continue to do so for $i \in [1; 100]$. DISTCOV, DISCORR and Hoeffding remain between 80% and 90%. HSIC and SH_MAXENT1 drop to $> 60\%$ after $i = 20$ and remain above 60% for $i < 100$. SH_MAXENT2, HSIC_IC and HSIC_IC2 drop to 50% for $i \in [20; 100]$.

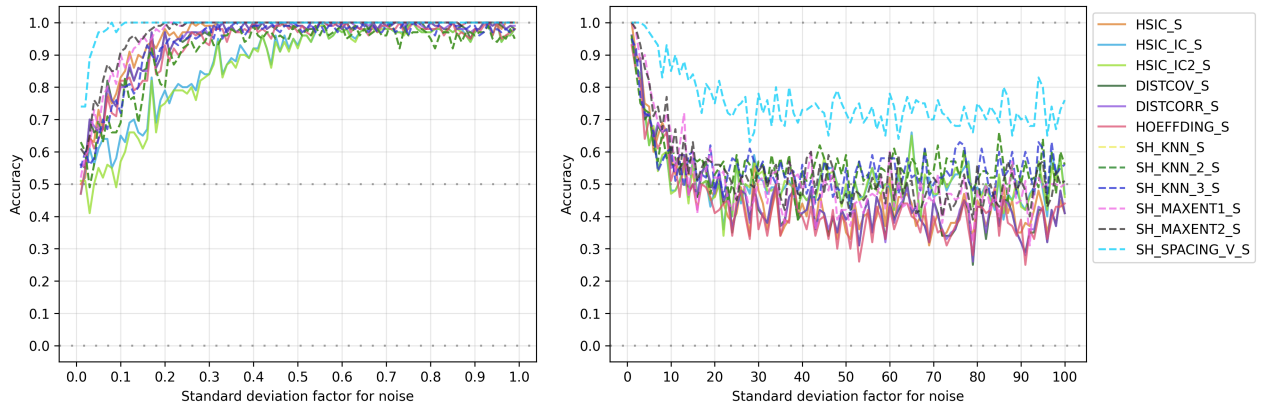


Figure 3.10: RESIT & different noise levels & decoupled estimation & $Y = \mathcal{U} + \mathcal{L}$

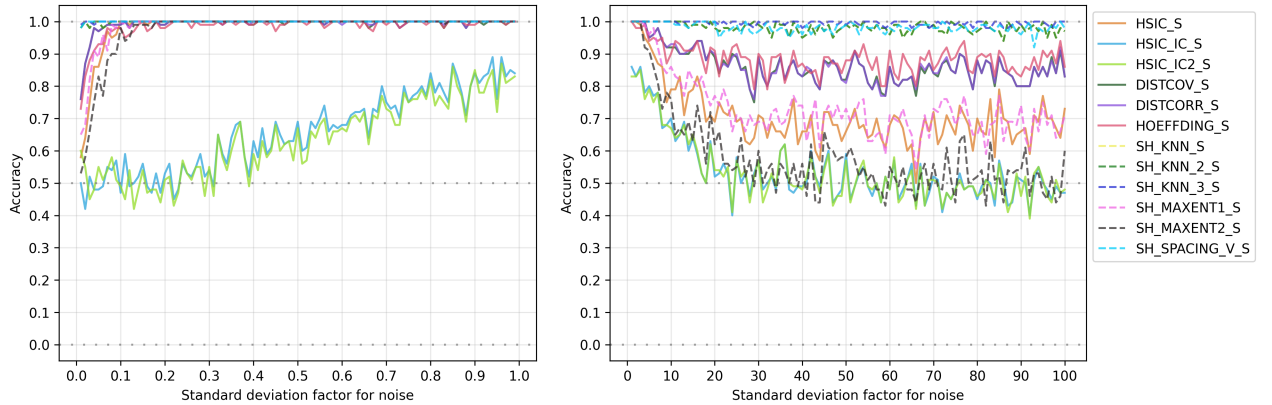


Figure 3.11: RESIT & different noise levels & decoupled estimation & $Y = \mathcal{U}^3 + \mathcal{U}$

Fig. 3.12 shows the non-linear model $Y = \mathcal{U}^3 + \mathcal{N}$. All estimators, except HSIC_IC and HSIC_IC2, remain above 95% for $i \in [0.05; 1]$ and for $i \in [1; 100]$ the estimators converge differently. All three Shannon differential entropy measures with kNNs and SH_SPACING_V remain above 95% accuracy. DISTCOV, DISCORR and HOEFFDING keep a mean of $\sim 85\%$ accuracy. HSIC and SH_MAXENT1 remain above 60% accuracy. SH_MAXENT2 is pretty much unidentifiable and HSIC_IC and HSIC_IC2 are unidentifiable for $i \in [0.01; 100]$. Fig. 3.13 shows the non-linear model $Y = \mathcal{U}^3 + \mathcal{L}$. The behaviour of different estimators is almost the same as for $Y = \mathcal{U}^3 + \mathcal{N}$. The only differences are that HSIC_IC performs slightly better for $i \in [0.2; 1]$ and DISTCOV, DISTCORR, HSIC and SH_MAXENT2 perform worse.

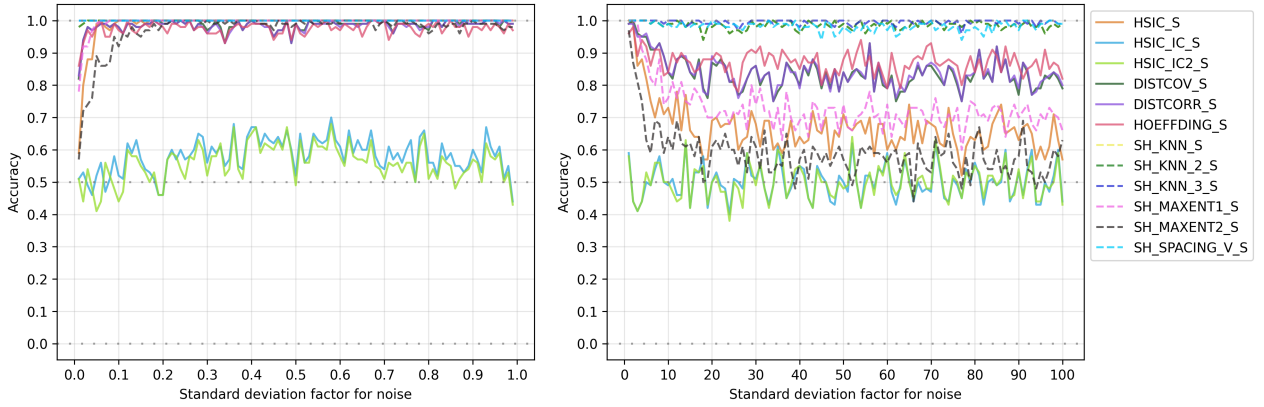


Figure 3.12: RESIT & different noise levels & decoupled estimation & $Y = \mathcal{U}^3 + \mathcal{N}$

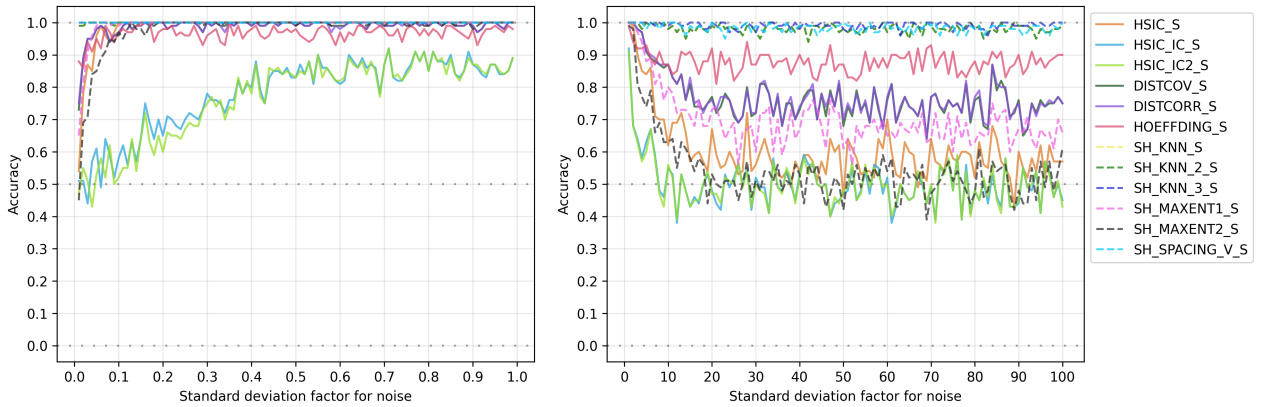


Figure 3.13: RESIT & different noise levels & decoupled estimation & $Y = \mathcal{U}^3 + \mathcal{L}$

Fig. 3.14 shows the linear model $Y = \mathcal{L} + \mathcal{L}$. First, for $i \in [0.4; 2]$ SH_MAXENT1 and SH_MAXENT2 have accuracy close to 100%. Next, for $i \in [0.4; 1]$ HSIC, HSIC_IC, HSIC_IC2, SH_SPACING_V, DISTCOV and DISTCORR remain above 90% accuracy. Hoeffding, and the three Shannon kNN estimators never reach an accuracy above 90%. After $i = 1$ all estimators drop fast towards 50%. Fig. 3.15 shows the linear model $Y = \mathcal{L} + \mathcal{N}$. This has a similar pattern as the previous one. For $i \in [0.3; 1]$ HSIC, SH_MAXENT1 and SH_MAXENT2 have accuracy greater than 90%. SH_SPACING_V, HSIC_IC, HSIC_IC2, DISTCOV and DISTCORR lie between 85% and 95% accuracy for $i \in [0.4; 1]$ and Hoeffding remains between 80% and 90%. Again, the three Shannon kNN estimators never reach an accuracy higher than 80%. After $i = 1$ all estimators drop fairly fast towards unidentifiability. Note: in Fig. 3.14 and Fig. 3.15 SH_KNN and SH_KNN_2 are overlapping completely.

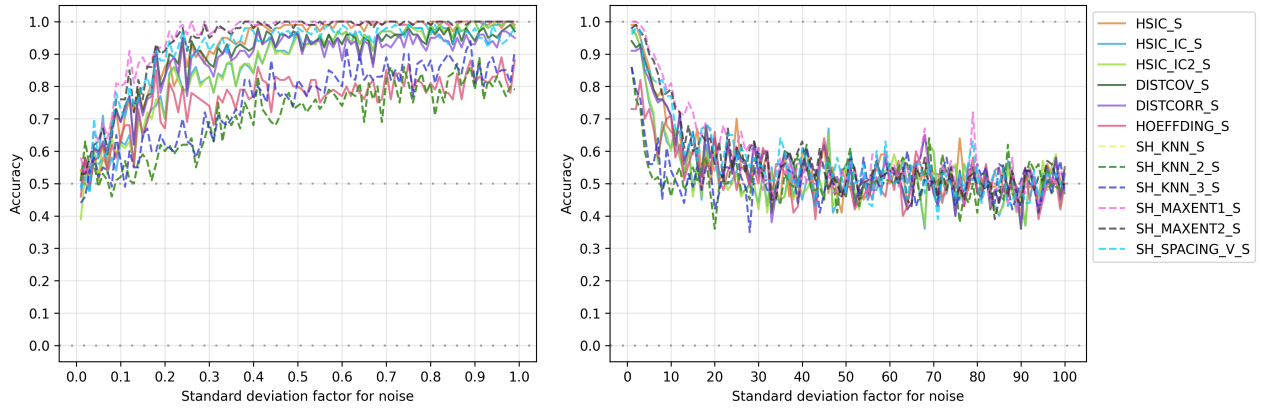


Figure 3.14: RESIT & different noise levels & decoupled estimation & $Y = \mathcal{L} + \mathcal{L}$

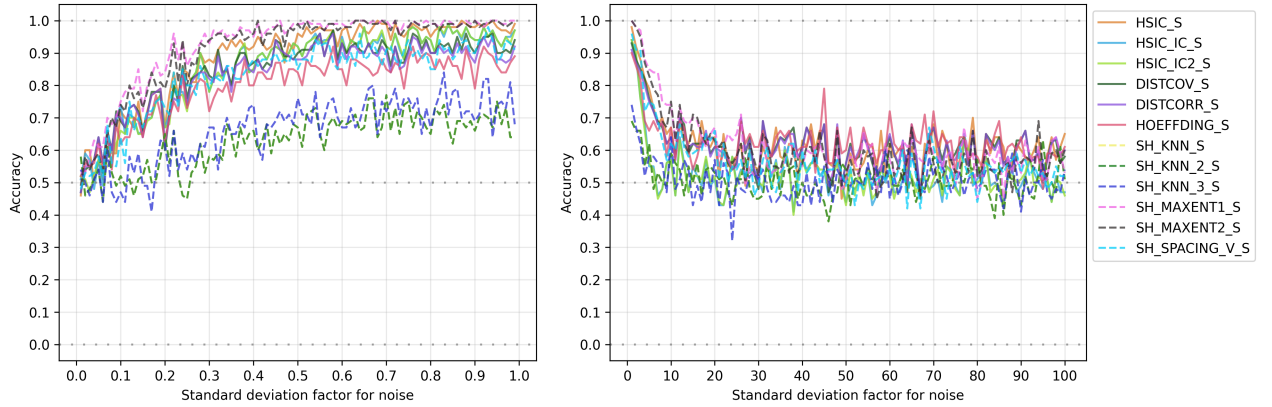


Figure 3.15: RESIT & different noise levels & decoupled estimation & $Y = \mathcal{L} + \mathcal{N}$

Fig. 3.16 shows the linear model $Y = \mathcal{L} + \mathcal{U}$. SH_SPACING_V performs the best of all estimators and has an accuracy of 100% for $i \in [0.5; 5]$. All other estimators slowly climb towards good identifiability and for $i \in [0.7; 7]$ they remain above 90% accuracy. Afterwards, all other estimators drop with similar pace towards unidentifiability. Fig. 3.17 shows the non-linear model $Y = \mathcal{L}^3 + \mathcal{L}$. This experiments shows the best results of all. For $i \in [0.1; 100]$ all estimators (except SH_MAXENT1 and SH_MAXENT2) have an accuracy 90% or higher SH_SPACING_V and the three Shannon kNN estimators have an accuracy of 100% for $i \in [0.01; 100]$. Only SH_MAXENT1 and SH_MAXENT2 perform bad at the beginning but still have an accuracy of 90% or higher for $i \in [0.35; 100]$.

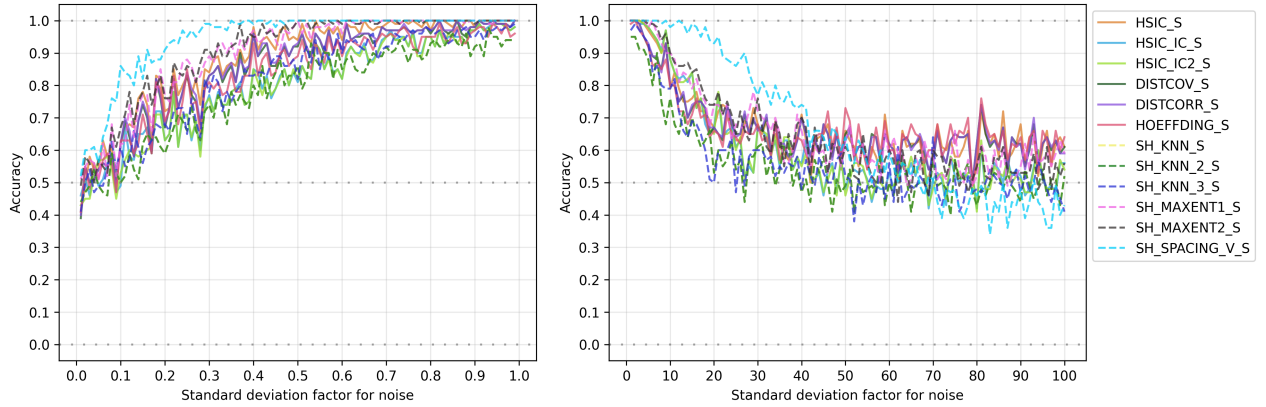


Figure 3.16: RESIT & different noise levels & decoupled estimation & $Y = \mathcal{L} + \mathcal{U}$

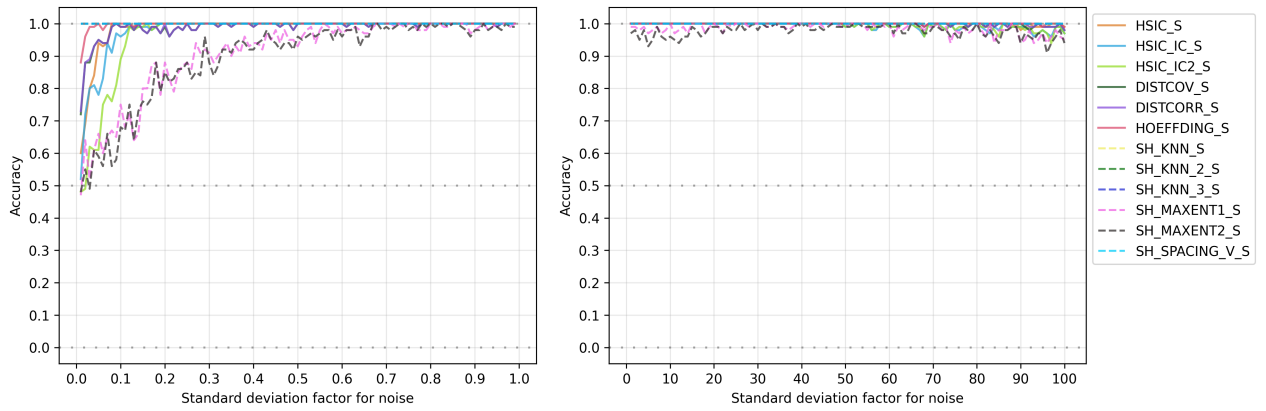


Figure 3.17: RESIT & different noise levels & decoupled estimation & $Y = \mathcal{L}^3 + \mathcal{L}$

Fig. 3.18 shows the non-linear model $Y = \mathcal{L}^3 + \mathcal{N}$. This shows similar results as Fig. 3.17. For $i \in [0.1; 100]$ all estimators (except SH_MAXENT1 and SH_MAXENT2) have an accuracy 90% or higher SH_SPACING_V and the three Shannon kNN estimators have an accuracy of 100% for $i \in [0.01; 100]$. Only SH_MAXENT1 and SH_MAXENT2 perform bad at the beginning but still have an accuracy of 90% or higher for $i \in [0.35; 100]$. Fig. 3.19 shows the non-linear model $Y = \mathcal{L}^3 + \mathcal{U}$. Similar as the two previous results. For $i \in [0.15; 100]$ all estimators (except SH_MAXENT1 and SH_MAXENT2) have an accuracy 90% or higher SH_SPACING_V, and the three Shannon kNN estimators have an accuracy of 100% for $i \in [0.01; 100]$. Only SH_MAXENT1 and SH_MAXENT2 perform bad at the beginning but still have an accuracy of 90% or higher for $i \in [0.7; 100]$. For $i \in [1; 100]$ all estimators are very close to 100% accuracy.

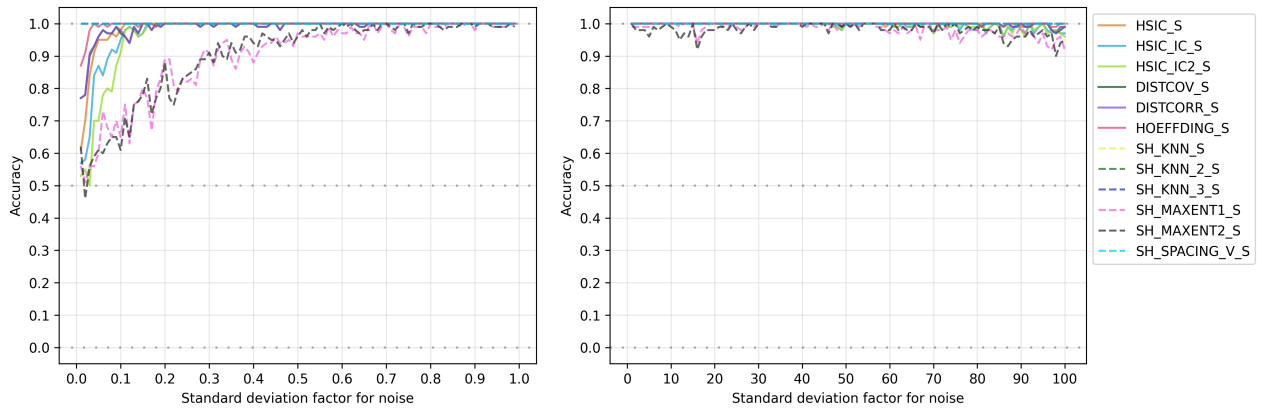


Figure 3.18: RESIT & different noise levels & decoupled estimation & $Y = \mathcal{L}^3 + \mathcal{N}$

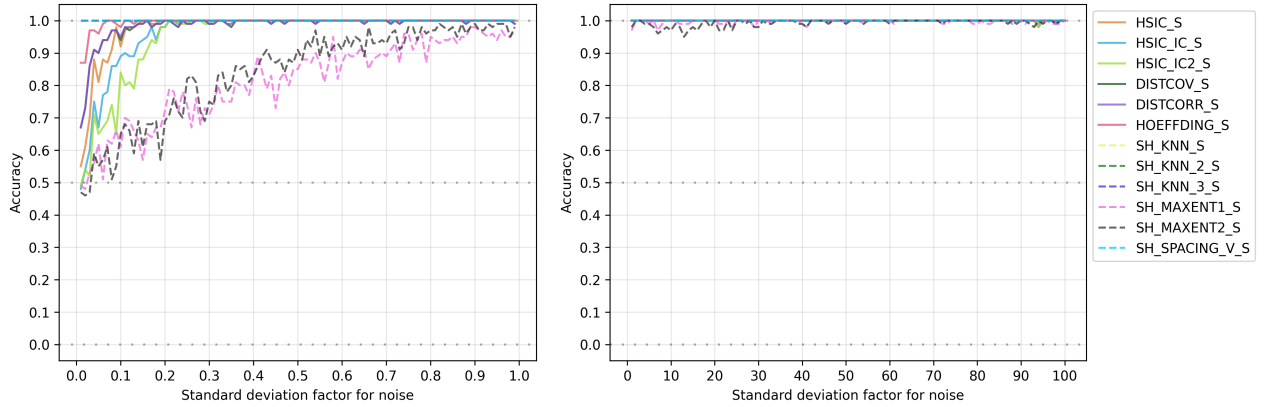


Figure 3.19: RESIT & different noise levels & decoupled estimation & $Y = \mathcal{L}^3 + \mathcal{U}$

Summary and Conclusion

Table 3.1 contains an overview of the results. The rows represent each structural equation and each column represents the estimator used. The values in the cells describe on what range of i the estimator *can* reach over 90%. Estimators have some variance in the results and thus on some intervals they fall below 90% accuracy. The limits in the cells were chosen as follows: the lower limit designates where estimators reaches the first time 90% or higher, and the upper limit designates the last time where it reaches 90% or higher. In between, most of the time estimators remain above 90% or rarely fall below, but not more than 10%. Empty cells mean that in that case the estimator never reached

90% or higher.

As the results show, different noise levels do have an impact on the identifiability performance in RESIT methods. In general the linear equation models are more fragile in RESIT than the non-linear equation models because non-linear relationships tend to break the symmetry between the variables easier, see Hoyer et al. (2009). Furthermore, in all cases the test results themselves have a standard deviation between 0.05 to 0.1 as one can see in the sharp wiggles in the plots.

Looking now only at the best estimation function and assuming a strong identifiability equal or greater than 90% accuracy then for all linear cases factor i is smaller than 10 (even smaller than 5 in some cases, e.g., Fig. 3.4) and bigger than 0.5. In other words, if $i \notin [0.5; 5]$ then the accuracy is below 90%. This looks different for the non-linear cases. For Fig. 3.6 e.g., accuracy is greater than 90% if $i \in [0.05; 100]$. Accuracy is even equal to 100% in the cases where $X \sim \mathcal{L}$ (Fig. 3.17 - Fig. 3.19) with $i \in [0.01; 100]$.

Some estimators perform differently depending on the setup. For example, in Fig. 3.11 - Fig. 3.13, the three Shannon differential entropy estimators with kNNs always perform above 90% accuracy for $i \in [0.01; 100]$ and even with 100% accuracy for $i \in [0.01; 100]$ in Fig. 3.17 - Fig. 3.19. At the same time, the HSIC with incomplete cholesky (HSIC_IC and HSIC_IC2) has the worst performance. There is even one case where HSIC_IC never achieves identifiability (Fig. 3.12). Overall, SH_SPACING_V performs the best in almost all cases, and is only outperformed by SH_MAXENT1 and SH_MAXENT2 in Fig. 3.4, Fig. 3.14 and Fig. 3.15. Some independence tests lose some of the accuracy while entropy estimators retain an accuracy over 90% (e.g., Fig. 3.11, Fig. 3.12 and Fig. 3.13). Additionally, it is worth to mention that entropy estimators are less computationally demanding than independence tests but can be quite sensitive to discretization effects Mooij et al. (2016). However, entropy estimators can only be used with the prior assumption we made: *there is only one causal direction and it is present in the model*. Section 3.3 contains experiments with the same setup but without this prior assumption.

In the next section, we compare decoupled estimation and coupled estimation.

Equation	HSIC	HISC	IC	HSIC	IC2	DISTCOV	DISTCORR	HOEFFDING	SH_KNN	SH_KNN_2	SH_KNN_3	SH_MAXENT1	SH_MAXENT2	SH_SPACING_V
$Y = N + N$														
$Y = N + U$	0.6 - 4	3 - 7		3 - 7		1	1				0.85 - 4	0.65 - 5	0.4 - 8	0.2 - 22
$Y = N + \mathcal{L}$	0.38 - 2	0.75 - 2		0.75 - 2		0.8 - 1	0.87 - 1					0.3 - 3	0.33 - 3	0.82 - 1
$Y = N^3 + N$	0.09 - 68	0.1 - 40		0.1 - 40		0.07 - 100	0.07 - 100	0.02 - 100	0.01 - 100	0.01 - 100	0.01 - 100	0.01 - 100	0.01 - 100	0.01 - 100
$Y = N^3 + U$	0.16 - 100	0.16 - 88		0.17 - 88		0.14 - 100	0.14 - 100	0.05 - 100	0.01 - 100	0.01 - 100	0.01 - 100	0.33 - 85	0.43 - 91	0.01 - 100
$Y = N^3 + \mathcal{L}$	0.11 - 70	0.1 - 35		0.1 - 35		0.08 - 88	0.05 - 88	0.04 - 100	0.01 - 100	0.01 - 100	0.01 - 100	0.18 - 67	0.25 - 65	0.01 - 100
$Y = U + U$	0.18 - 6	3		3		0.2 - 3	0.2 - 3	0.2 - 3	0.2 - 3	0.2 - 2	0.2 - 3	0.23 - 3	0.12 - 8	0.05 - 21
$Y = U + N$	0.21 - 1					0.25 - 1	0.25 - 1	1	0.26 - 1	0.26 - 1	0.2 - 1	0.2 - 1	0.1 - 4	0.04 - 9
$Y = U + \mathcal{L}$	0.15 - 1	0.35 - 1		0.35 - 1		0.2 - 1	0.2 - 1	0.15 - 1	0.21 - 1	0.21 - 1	0.16 - 1	0.12 - 3	0.1 - 3	0.03 - 8
$Y = U^8 + U$	0.05 - 6					0.03 - 20	0.03 - 20	0.03 - 100	0.01 - 100	0.01 - 100	0.01 - 100	0.05 - 7	0.09 - 5	0.01 - 100
$Y = U^8 + N$	0.04 - 3					0.01 - 85	0.01 - 85	0.01 - 95	0.01 - 100	0.01 - 100	0.01 - 100	0.02 - 4	0.08 - 2	0.01 - 100
$Y = U^8 + \mathcal{L}$	0.05 - 3	0.7 - 1		0.7 - 1		0.02 - 5	0.02 - 5	0.02 - 100	0.01 - 100	0.01 - 100	0.01 - 100	0.03 - 4	0.06 - 3	0.01 - 100
$Y = \mathcal{L} + \mathcal{L}$	0.3 - 5	0.4 - 4		0.4 - 4		0.23 - 4	0.23 - 4				0.6 - 1	0.2 - 6	0.17 - 5	0.17 - 4
$Y = \mathcal{L} + N$	0.32 - 3	0.36 - 3		0.36 - 3		0.33 - 2	0.33 - 2	0.57 - 1				0.21 - 4	0.21 - 4	0.49 - 4
$Y = \mathcal{L} + U$	0.4 - 8	0.6 - 7		0.6 - 7		0.4 - 5	0.4 - 5	0.4 - 5	0.53 - 4	0.53 - 4	0.51 - 5	0.32 - 10	0.32 - 10	0.16 - 27
$Y = \mathcal{L}^3 + \mathcal{L}$	0.05 - 100	0.06 - 100		0.1 - 100		0.03 - 100	0.03 - 100	0.01 - 100	0.01 - 100	0.01 - 100	0.01 - 100	0.26 - 100	0.28 - 100	0.01 - 100
$Y = \mathcal{L}^3 + N$	0.04 - 100	0.07 - 100		0.1 - 100		0.03 - 100	0.03 - 100	0.02 - 100	0.01 - 100	0.01 - 100	0.01 - 100	0.28 - 100	0.3 - 100	0.01 - 100
$Y = \mathcal{L}^3 + U$	0.07 - 100	0.12 - 100		0.15 - 100		0.04 - 100	0.04 - 100	0.02 - 100	0.01 - 100	0.01 - 100	0.01 - 100	0.53 - 100	0.43 - 100	0.01 - 100

Table 3.1: Summary Table for RESTT & different noise levels & Decoupled estimation. The numbers reflect the ranges of noise that allow identifiability with accuracy around 90%.

3.2 RESIT with Different Noise Levels and coupled estimation

In the previous section, Section 3.1, we discussed decoupled estimation when data was split into training (80%) and testing (20%) sets. The reason one would want to split data is of computational nature: smaller sets of samples allow for faster computation of the estimates, notably the independence estimators, but might decrease the accuracy of the algorithm. The same data can be analyzed using the coupled estimation method when the entire set of 1000 samples is used for both the regression step and the estimation step, and in this case we achieve higher accuracy (or overall performance of the algorithm). Therefore, choosing between decoupled and coupled estimation is a trade-off between identifiability performance and computation speed. In this section we analyze the performance of RESIT for this setup. As the experimental procedure and the setup stay the same as in Section 3.1, we directly proceed to the discussion of results.

3.2.1 Results

The figures for the results here are to be interpreted in the same way as in the section before (see Section 3.1.3).

Individual Analysis

Again, reading individual results is not necessary as we provide an summary table in the summary section (Table 3.2).

Fig. 3.20 is the only case which remains unchanged performance wise ($Y = \mathcal{N} + \mathcal{N}$). Fig. 3.21 shows the linear model with $Y = \mathcal{N} + \mathcal{U}$. All estimators reach now an accuracy close to 100% at some interval $i \in [0.8; 5]$. The accuracy in the $[0.01; 1]$ interval climbs now faster for all estimators and drops more slowly for $i \in [1; 100]$.

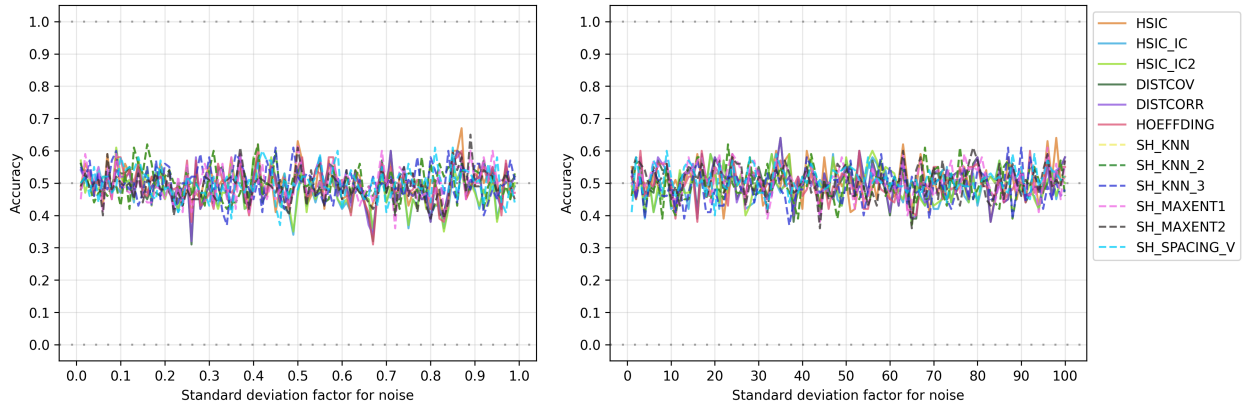


Figure 3.20: RESIT & different noise levels & coupled estimation & $Y = \mathcal{N} + \mathcal{N}$

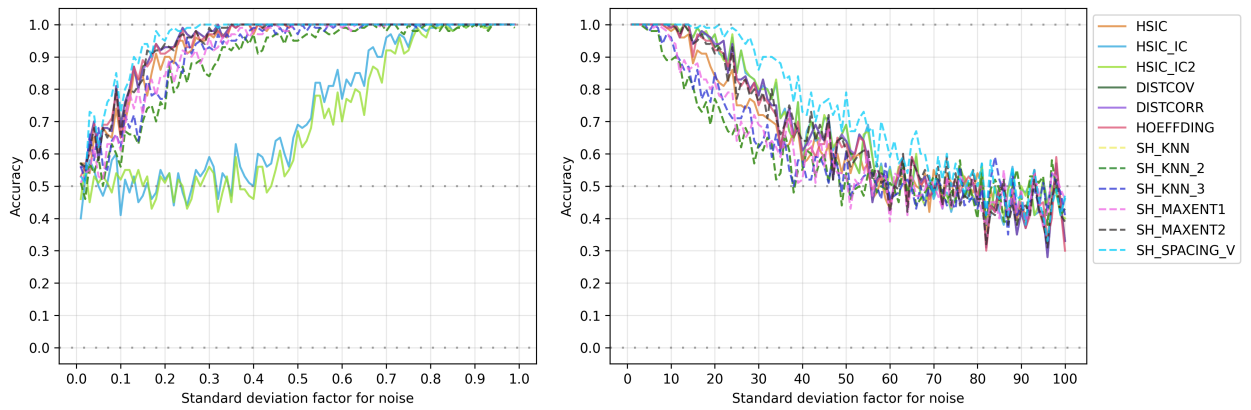


Figure 3.21: RESIT & different noise levels & coupled estimation & $Y = \mathcal{N} + \mathcal{U}$

Fig. 3.22 shows the linear model $Y = \mathcal{N} + \mathcal{L}$. All estimators except for the three Shannon kNN estimators now reach an accuracy close to 100% for $i \in [0.42; 5]$. The three kNN estimators achieve better performance than in the decoupled estimation but remain worse than the other estimators. Fig. 3.23 shows the non-linear model $Y = \mathcal{N}^3 + \mathcal{N}$. Here all estimators perform very good with $i \in [0.15; 50]$ having an accuracy close to 100%. With $i < 0.1$ most estimators drop fast below 90% accuracy. For $i > 50$ most estimators remain above 90% accuracy, except SH_MAXENT2, HSIC_IC and HSIC_IC2 which still remain above 80% accuracy.

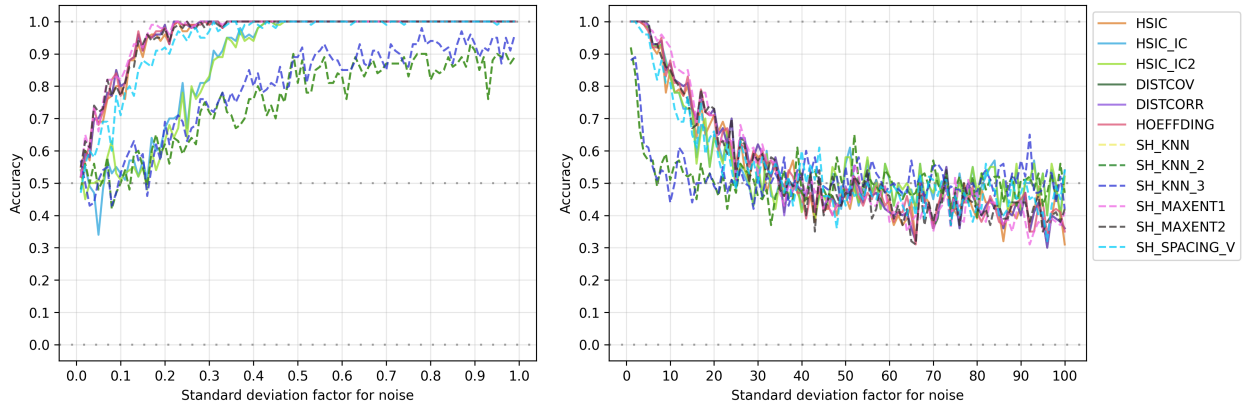


Figure 3.22: RESIT & different noise levels & coupled estimation & $Y = \mathcal{N} + \mathcal{L}$

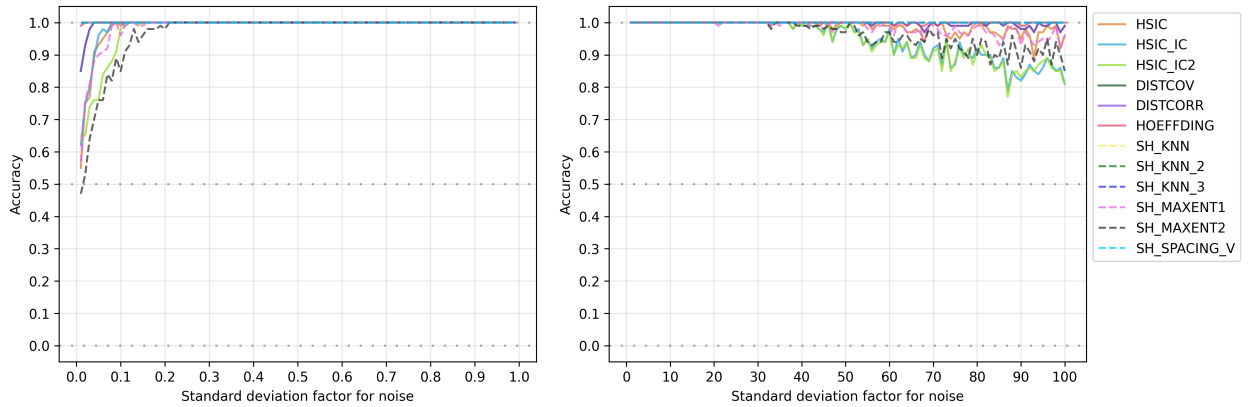


Figure 3.23: RESIT & different noise levels & coupled estimation & $Y = \mathcal{N}^3 + \mathcal{N}$

Fig. 3.24 shows the non-linear model $Y = \mathcal{N}^3 + \mathcal{U}$. This result is similar as the previous one. With $i \in [0.2; 100]$ we have accuracy close to 100% for all estimators. SH_MAXENT1 and SH_MAXENT2 now perform almost as good as other estimators for $i < 0.4$. Fig. 3.25 shows the non-linear model $Y = \mathcal{N}^3 + \mathcal{L}$. For $i \in [0.17; 40]$ all estimators are close to or at 100% accuracy. SH_MAXENT1 and SH_MAXENT2 perform as good as other estimators for $i < 0.2$. and $i > 60$. The accuracy for HSIC_IC and HSIC_IC2 still drops fairly far after $i > 50$ compared to the rest.

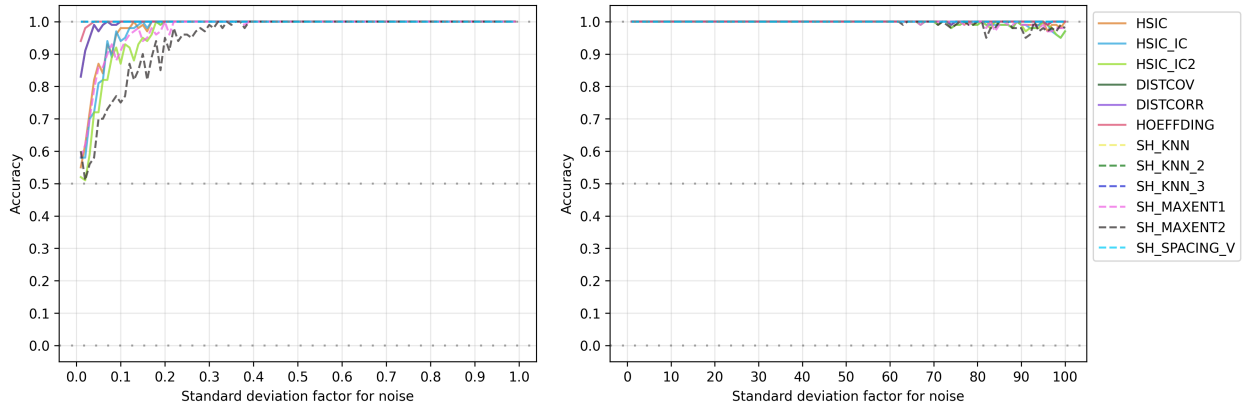


Figure 3.24: RESIT & different noise levels & coupled estimation & $Y = \mathcal{N}^3 + \mathcal{U}$

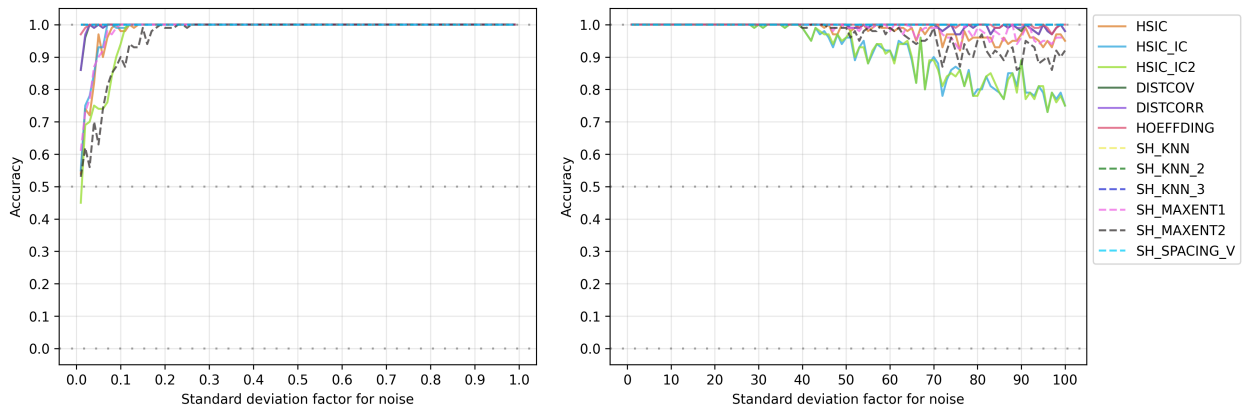


Figure 3.25: RESIT & different noise levels & coupled estimation & $Y = \mathcal{N}^3 + \mathcal{L}$

Fig. 3.26 shows the linear model $Y = \mathcal{U} + \mathcal{U}$. This shows some interesting changes. In the decoupled estimation HSIC_IC and HSIC_IC2 never reached a consistent range with accuracy above 90% but in the coupled estimation they do now. All estimators have an accuracy of 100% for $i \in [0.25; 5]$. Interestingly, SH_SPACING_V does not converge to 50%. HSIC_IC and HSIC_IC2 do clearly fall below 40% for $i > \sim 85$. (Note that 0% accuracy means that the wrong direction ($Y \rightarrow X$) is consistently identified.) Fig. 3.27 shows the linear model $Y = \mathcal{U} + \mathcal{N}$. For $i \in [0.2; 1]$ all estimators are close to or at 100% accuracy. In the decoupled estimation only two estimators were close to 100% accuracy in that interval. After $i = 1$ most estimators converge towards $\sim 60\%$ accuracy. HSIC_IC and HSIC_IC2 completely drop to unidentifiability. SH_SPACING_V remains above 90% accuracy for $i \in [1; 100]$.

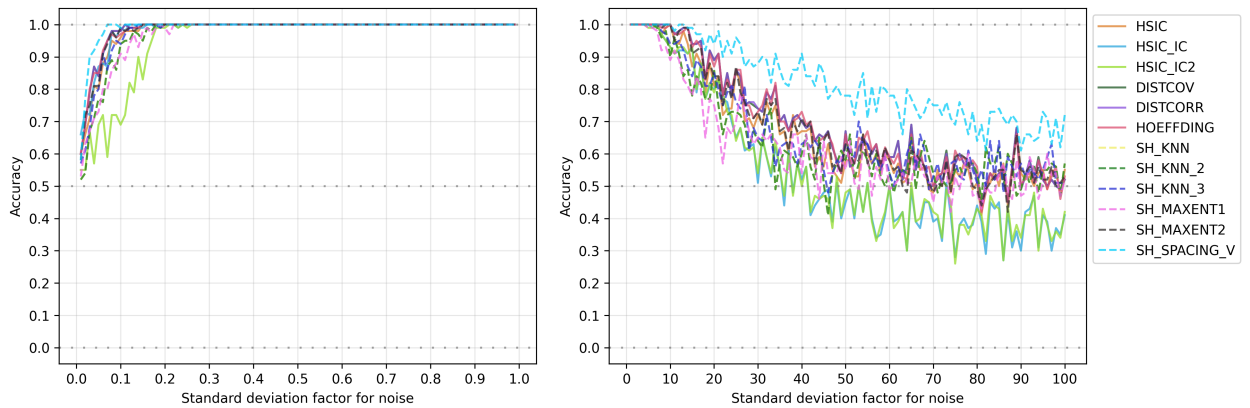


Figure 3.26: RESIT & different noise levels & coupled estimation & $Y = \mathcal{U} + \mathcal{U}$

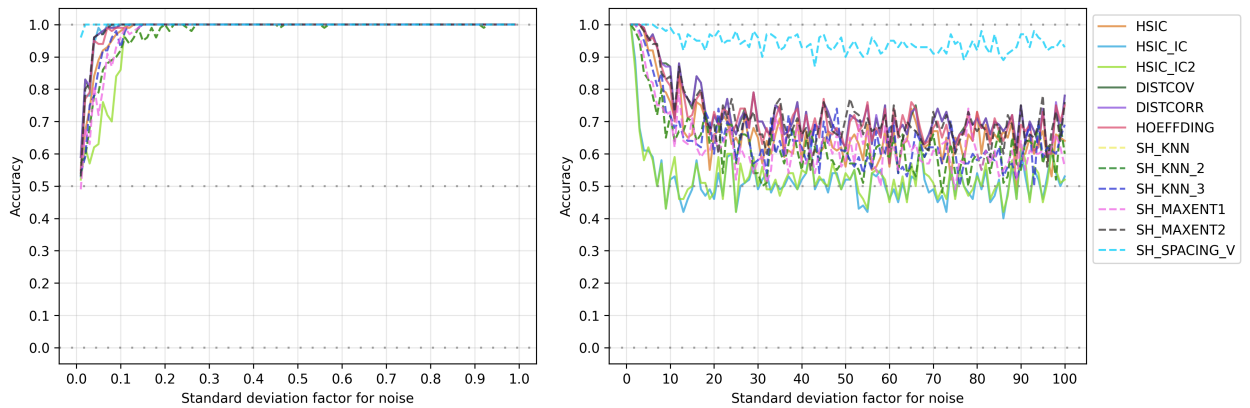


Figure 3.27: RESIT & different noise levels & coupled estimation & $Y = \mathcal{U} + \mathcal{N}$

Fig. 3.28 shows the linear model $Y = \mathcal{U} + \mathcal{L}$. This case has similar results as the previous one. For $i \in [0.1; 3]$ all estimators are close to or at 100% accuracy. SH_SPACING_V remains again over 90% accuracy for $i \in [1; 100]$. All other converge towards unidentifiability while the three Shannon kNN estimators converge towards 60% accuracy. Fig. 3.29 shows the non-linear model $Y = \mathcal{U}^3 + \mathcal{U}$. HSIC_IC and HSIC_IC2 now perform better and are close to 100% accuracy for $i \in [0.3; 5]$ while others have highest accuracy for $i \in [0.05; 5]$. For i larger than 5, results look similar to the decoupled estimation but overall the performance increased by an additive 5 – 15% for the various estimators. The exception again is HSIC_IC and HSIC_IC2 which lie clearly below 50% accuracy now.

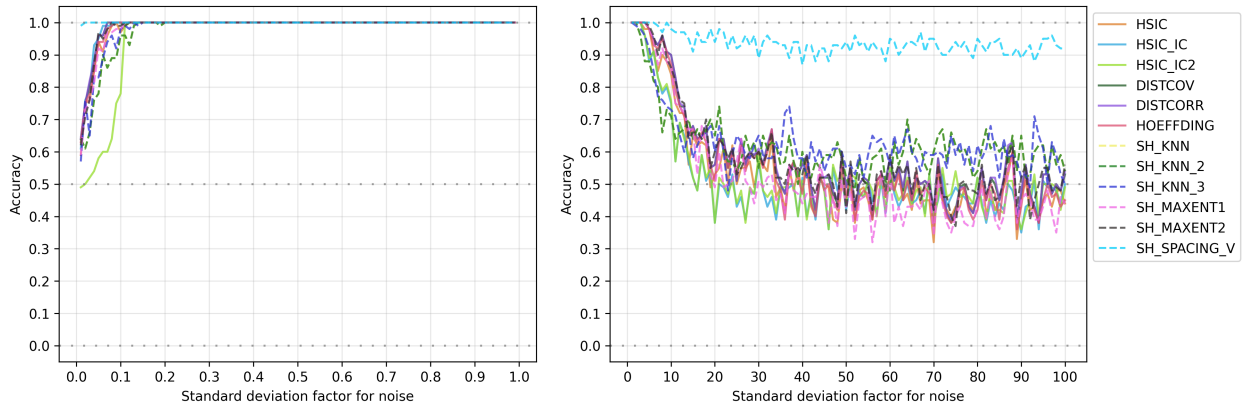


Figure 3.28: RESIT & different noise levels & coupled estimation & $Y = \mathcal{U} + \mathcal{L}$

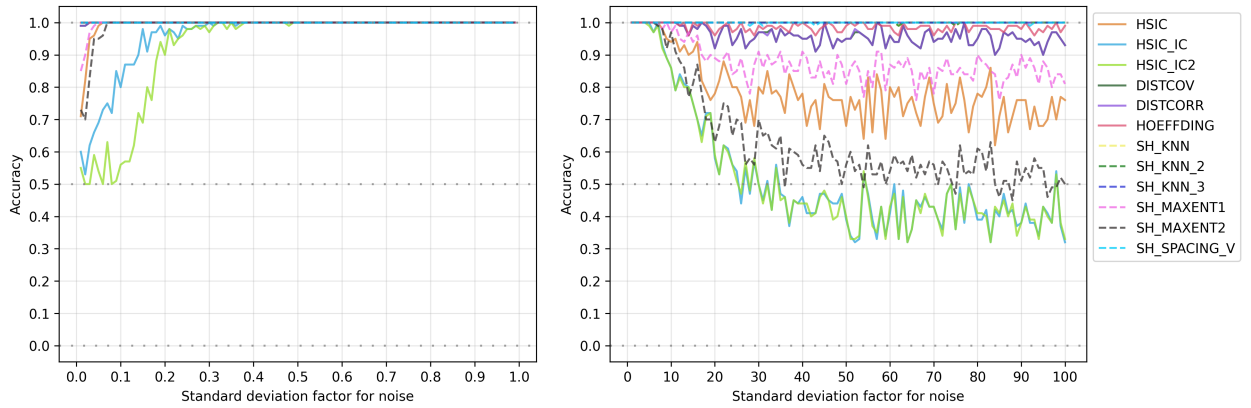


Figure 3.29: RESIT & different noise levels & coupled estimation & $Y = \mathcal{U}^3 + \mathcal{U}$

Fig. 3.30 shows the non-linear model $Y = \mathcal{U}^3 + \mathcal{N}$. In the decoupled estimation HSIC_IC and HSIC_IC2 never reached identifiability. This is now different for the coupled estimation: for $i \in [0.1; 0.75]$ they are both above 90% accuracy but begin to drop already after $i = 0.75$ towards unidentifiability. SH_SPACING_V and the three Shannon kNN estimators have perfect accuracy for $i \in [0.01; 100]$. All other estimators have their accuracy increased additively by 5–20% for i larger than 1. Fig. 3.31 shows the non-linear model $Y = \mathcal{U}^3 + \mathcal{L}$. This is similar to the previous case. SH_SPACING_V and the three Shannon kNN estimators are at 100% accuracy for $i \in [0.01; 100]$. All others reach 100% accuracy for $i \in [0.25; 1]$ and for $i > 1$ their accuracy have increased by an additive 5 – 20%.

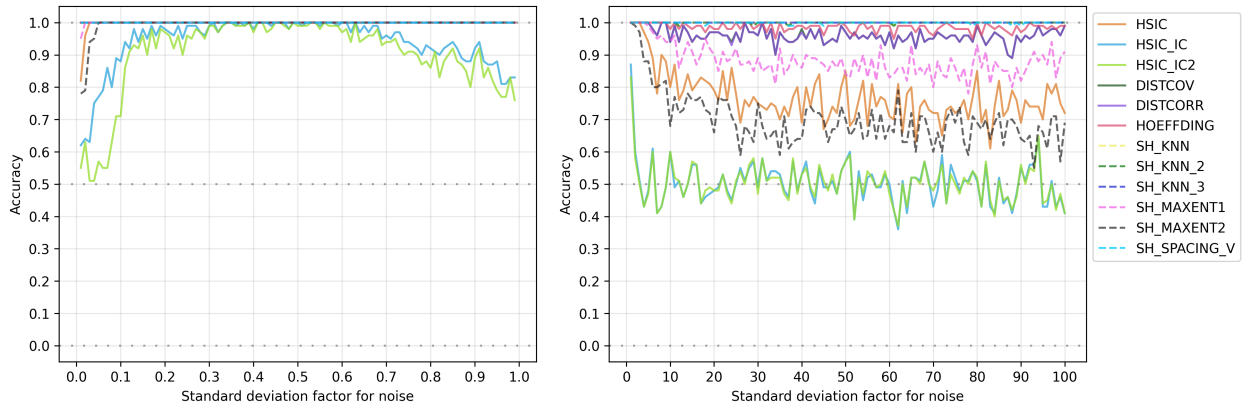


Figure 3.30: RESIT & different noise levels & coupled estimation & $Y = \mathcal{U}^3 + \mathcal{N}$

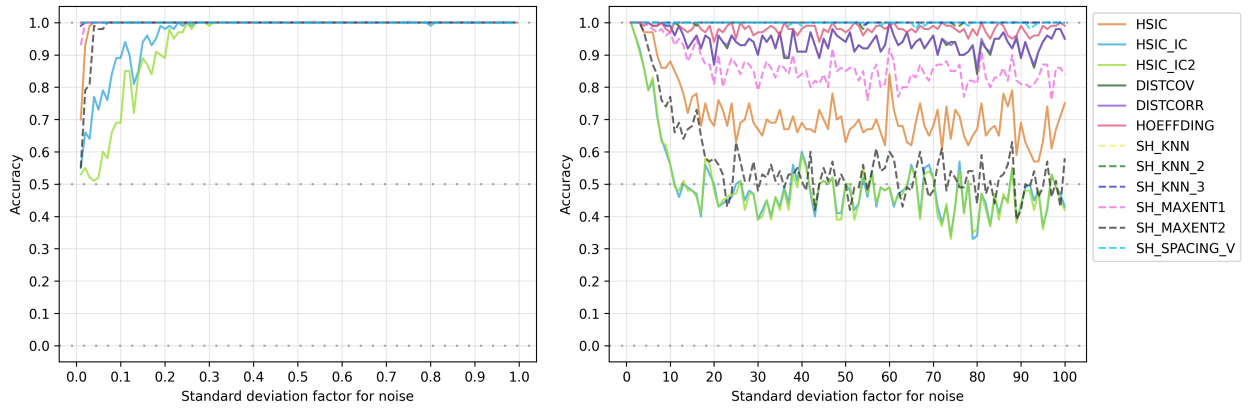


Figure 3.31: RESIT & different noise levels & coupled estimation & $Y = \mathcal{U}^3 + \mathcal{L}$

Fig. 3.32 shows the linear model $Y = \mathcal{L} + \mathcal{L}$. For $i \in [0.01; 1]$ estimators have improved significantly. The three Shannon kNN estimators still perform worse than other estimators, but they do reach now accuracy above 90% for $i \in [0.45; 1]$. All other estimators are close to or at 100% for $i \in [0.2; 5]$. Fig. 3.33 shows the linear model $Y = \mathcal{L} + \mathcal{N}$. This has a similar pattern as the previous one. The three Shannon kNN estimators still perform worse than other estimators and they barely reach 90% accuracy for $i = 1$. All other estimators are now close to or at 100% for $i \in [0.25; 5]$.

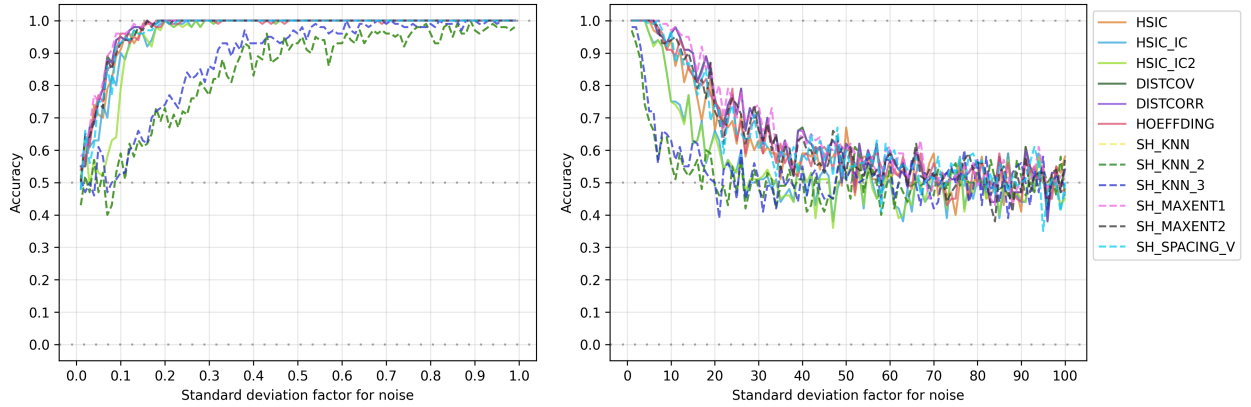


Figure 3.32: RESIT & different noise levels & coupled estimation & $Y = \mathcal{L} + \mathcal{L}$

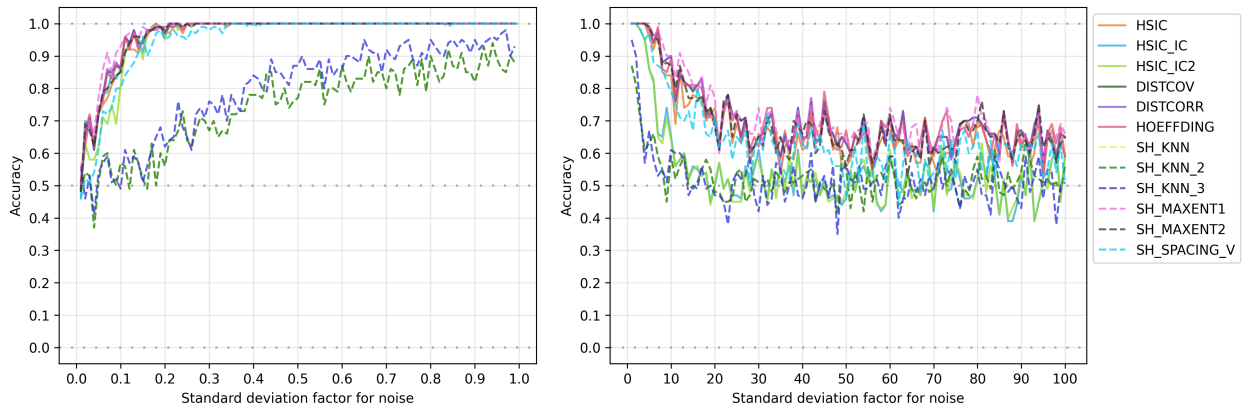


Figure 3.33: RESIT & different noise levels & coupled estimation & $Y = \mathcal{L} + \mathcal{N}$

Fig. 3.34 shows the linear model $Y = \mathcal{L} + \mathcal{U}$. While SH_SPACING_V performed the best of all estimators in the decoupled estimation most estimators are now close to the performance of SH_SPACING_V or even better. For $i \in [0.4; 5]$ all estimators have an accuracy close to or at 100%. Fig. 3.35 shows the non-linear model $Y = \mathcal{L}^3 + \mathcal{L}$. For $i \in [0.2; 100]$ all estimators are now close to or at 100% accuracy.

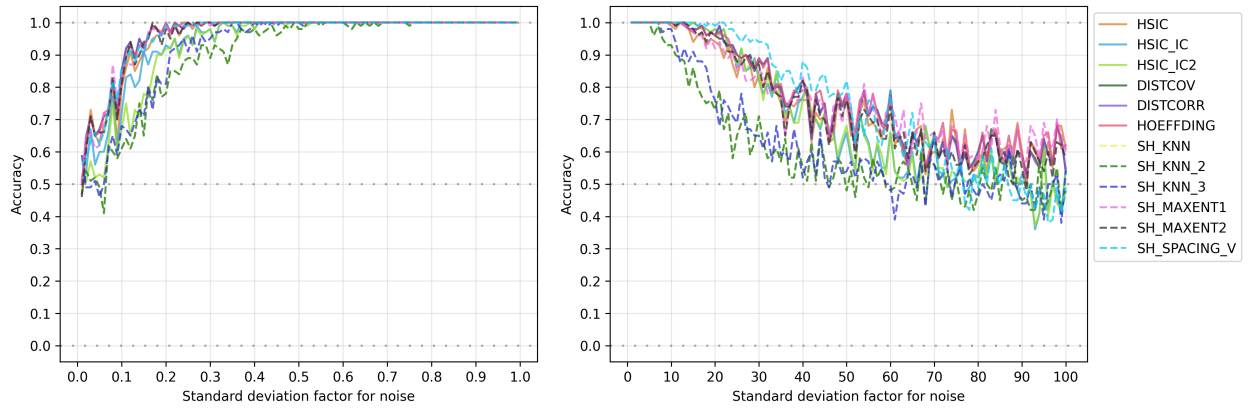


Figure 3.34: RESIT & different noise levels & coupled estimation & $Y = \mathcal{L} + \mathcal{U}$

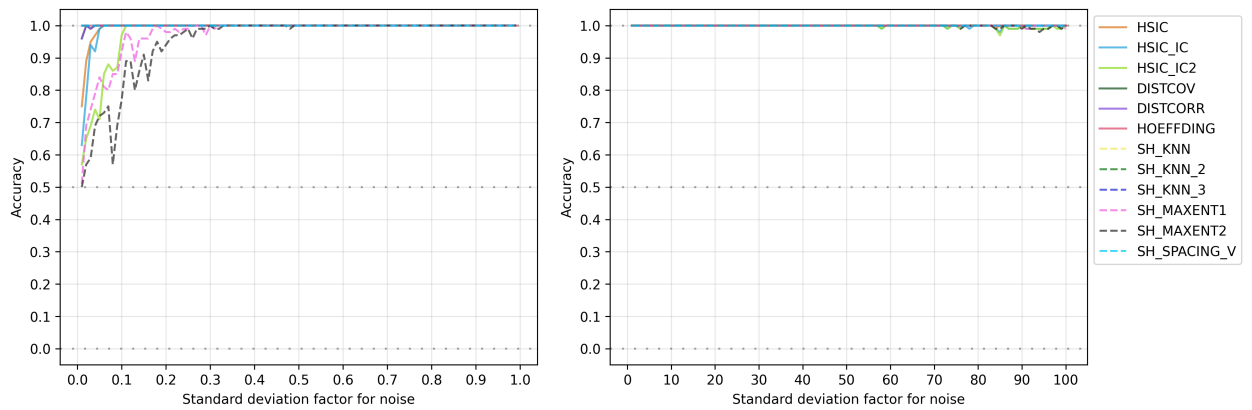


Figure 3.35: RESIT & different noise levels & coupled estimation & $Y = \mathcal{L}^3 + \mathcal{L}$

Fig. 3.36 shows the non-linear model $Y = \mathcal{L}^3 + \mathcal{N}$. Same as Fig. 3.17. For $i \in [0.2; 100]$ all estimators are now close to or at 100% accuracy. Fig. 3.37 shows the non-linear model $Y = \mathcal{L}^3 + \mathcal{U}$. Similar as the two previous results. SH_MAXENT1 and SH_MAXENT2 do perform better now but are still worse than all other estimators which, for $i \in [0.1; 100]$, are now close to or at 100% accuracy.

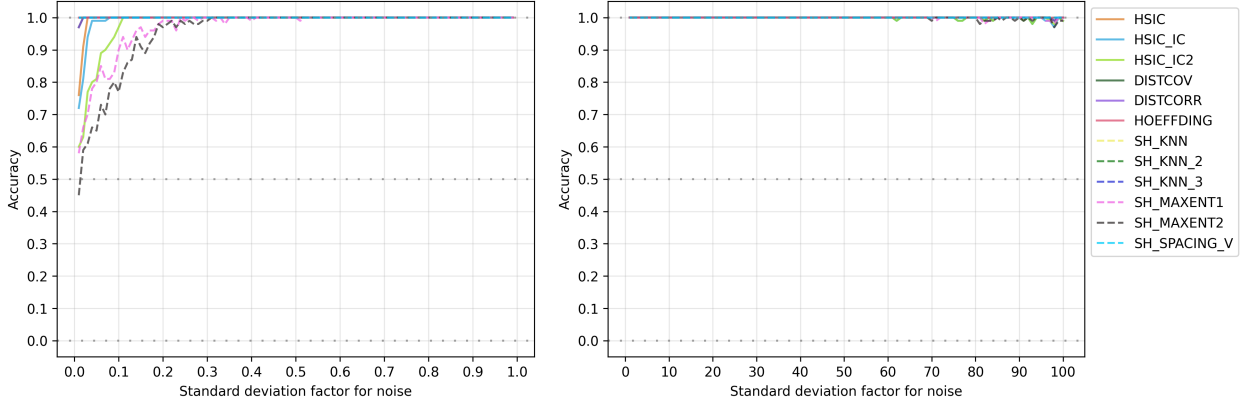


Figure 3.36: RESIT & different noise levels & coupled estimation & $Y = \mathcal{L}^3 + \mathcal{N}$

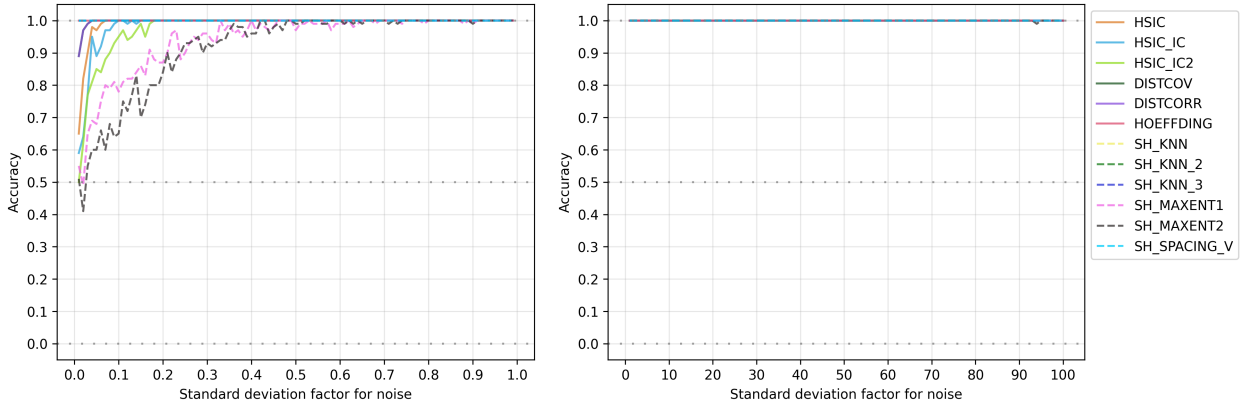


Figure 3.37: RESIT & different noise levels & coupled estimation & $Y = \mathcal{L}^3 + \mathcal{U}$

Summary and Conclusion

Table 3.2 follows the same scheme as Table 3.1. Similar to the previous section, different noise levels do have an impact on the identifiability performance of RESIT methods. Overall, all estimators perform better than in the decoupled estimation case. Some estimators show better performance in particular structural causal models (e.g., SH_SPACING_V in Fig. 3.27). Others do perform worse than the rest of the used estimators (e.g., HSIC_IC and HSIC_IC2 in Fig. 3.21). For all non-linear equation models the SH_SPACING_V and the three Shannon kNN estimators are always at or at least very close to 100% accuracy for $i \in [0.01; 100]$. SH_SPACING_V also keeps its good performance in the linear equation models. For the independence measures HSIC, DISTCOV, DISTCORR and Hoeffding perform quite similar and good overall. Furthermore, for linear equation models if the standard deviation of the noise term is smaller than the standard deviation of the independent variable (X) then RESIT is strong for $i \in [\sim 0.2; 1]$. In the opposite direction, when the standard deviation of the noise term is larger, RESIT does not perform that well. Often it is only robust up to a factor $i = 10$

(e.g., Fig. 3.22). Note again that this results are also based on the assumption that in our bivariate structure only one and exact one direction of cause and effect is present (namely $X \rightarrow Y$). Therefore, without this assumption we cannot compare the estimates directly but rather need to compare the estimate to a derived p-value given some value of alpha (e.g., commonly $\alpha = 0.05$). The next section describes experiments and results without this assumption.

Equation	HSIC	HISC	IG	HSIC	IC2	DISTCOV	DISTCORR	HOEFFDING	SH	KNN	SH	KNN	2	SH	KNN	3	SH	MAXENT1	SH	MAXENT2	SH	SPACING	V
$Y = N + N$	0.17 - 18	0.65 - 26	0.7 - 26	0.16 - 23	0.16 - 23	0.16 - 23	0.16 - 23	0.16 - 25	0.32 - 12	0.32 - 12	0.24 - 12	0.23 - 12	0.15 - 22	0.13 - 33									
$Y = N + U$	0.13 - 8	0.31 - 7	0.33 - 7	0.13 - 7	0.13 - 8	0.13 - 8	0.13 - 8	0.16 - 25	0.76 - 1	0.76 - 1	0.51 - 1	0.12 - 10	0.13 - 7										
$Y = N + \mathcal{L}$	0.04 - 100	0.04 - 83	0.08 - 83	0.02 - 100	0.02 - 100	0.02 - 100	0.01 - 100	0.01 - 100	0.01 - 100	0.01 - 100	0.01 - 100	0.05 - 100	0.11 - 98										
$Y = N^3 + N$	0.08 - 100	0.06 - 100	0.08 - 100	0.02 - 100	0.02 - 100	0.02 - 100	0.01 - 100	0.01 - 100	0.01 - 100	0.01 - 100	0.01 - 100	0.06 - 100	0.16 - 100										
$Y = N^3 + U$	0.04 - 100	0.04 - 70	0.09 - 70	0.02 - 100	0.02 - 100	0.02 - 100	0.01 - 100	0.01 - 100	0.01 - 100	0.01 - 100	0.01 - 100	0.05 - 100	0.1 - 100										
$Y = N^3 + \mathcal{L}$	0.06 - 16	0.06 - 15	0.14 - 15	0.05 - 21	0.05 - 21	0.05 - 21	0.05 - 21	0.05 - 21	0.07 - 12	0.07 - 12	0.07 - 14	0.1 - 12	0.03 - 40										
$Y = U + U$	0.05 - 6	0.04 - 3	0.1 - 3	0.04 - 7	0.04 - 7	0.04 - 7	0.04 - 7	0.04 - 7	0.08 - 4	0.08 - 4	0.05 - 5	0.06 - 4	0.03 - 7										
$Y = U + N$	0.04 - 7	0.04 - 5	0.11 - 5	0.04 - 10	0.04 - 10	0.04 - 10	0.04 - 10	0.04 - 8	0.09 - 4	0.09 - 4	0.05 - 5	0.04 - 8	0.04 - 8										
$Y = U + \mathcal{L}$	0.03 - 16	0.14 - 13	0.17 - 13	0.01 - 100	0.01 - 100	0.01 - 100	0.01 - 100	0.01 - 100	0.01 - 100	0.01 - 100	0.01 - 100	0.02 - 90	0.04 - 12										
$Y = U^8 + U$	0.02 - 6	0.1 - 0.92	0.12 - 0.91	0.01 - 100	0.01 - 100	0.01 - 100	0.01 - 100	0.01 - 100	0.01 - 100	0.01 - 100	0.01 - 100	0.01 - 100	0.03 - 4										
$Y = U^8 + N$	0.03 - 7	0.1 - 4	0.17 - 4	0.01 - 100	0.01 - 100	0.01 - 100	0.01 - 100	0.01 - 100	0.01 - 100	0.01 - 100	0.01 - 100	0.01 - 88	0.04 - 5										
$Y = U^8 + \mathcal{L}$	0.1 - 13	0.1 - 8	0.12 - 8	0.08 - 15	0.08 - 15	0.08 - 15	0.08 - 15	0.1 - 10	0.37 - 3	0.37 - 3	0.32 - 4	0.07 - 17	0.1 - 13										
$Y = \mathcal{L} + \mathcal{L}$	0.1 - 7	0.1 - 4	0.1 - 4	0.1 - 7	0.1 - 7	0.1 - 7	0.1 - 7	0.1 - 7	0.61 - 1	0.61 - 1	0.37 - 3	0.07 - 13	0.1 - 7										
$Y = \mathcal{L} + U$	0.12 - 23	0.14 - 26	0.14 - 26	0.1 - 25	0.1 - 25	0.1 - 25	0.1 - 25	0.1 - 25	0.27 - 12	0.27 - 12	0.21 - 15	0.11 - 24	0.11 - 23										
$Y = \mathcal{L} + \mathcal{L}$	0.02 - 100	0.03 - 100	0.09 - 100	0.01 - 100	0.01 - 100	0.01 - 100	0.01 - 100	0.01 - 100	0.01 - 100	0.01 - 100	0.01 - 100	0.1 - 100	0.15 - 100										
$Y = \mathcal{L}^3 + N$	0.02 - 100	0.03 - 100	0.7 - 100	0.01 - 100	0.01 - 100	0.01 - 100	0.01 - 100	0.01 - 100	0.01 - 100	0.01 - 100	0.01 - 100	0.1 - 100	0.14 - 100										
$Y = \mathcal{L}^3 + U$	0.04 - 100	0.05 - 100	0.07 - 100	0.01 - 100	0.01 - 100	0.01 - 100	0.01 - 100	0.01 - 100	0.01 - 100	0.01 - 100	0.01 - 100	0.17 - 100	0.21 - 100										

Table 3.2: Summary Table for RESIT & different noise levels & Coupled estimation. The numbers reflect the ranges of noise that allow identifiability with accuracy around 90%.

3.3 RESIT with Different Noise Levels without prior assumption

Without assuming that exactly one direction has to be present in our bivariate model, we must then account for four different possibilities instead:

1. $X \rightarrow Y$ and $Y \not\rightarrow X$
2. $X \rightarrow Y$ and $Y \rightarrow X$
3. $X \rightarrow Y$ and $Y \rightarrow X$
4. $X \not\rightarrow Y$ and $Y \not\rightarrow X$

This means that we cannot compare estimates directly but have to estimate an α value for the independence test when testing each direction and we can no longer use entropy estimators.

3.3.1 Setup

This setup is the same as in Section 3.1.1. The only difference is a small modification in the algorithm we use (Algorithm 1). More precisely, the first steps remain unchanged but the step number 5 needs to be adjusted. Here, we perform independence test on the independent variable and the residuals and compare the independence estimate to the alpha estimate with $\alpha = 0.05$. Furthermore, since the equation of our data is $Y = X + N_y$ only the outcome $X \rightarrow Y$ and $Y \not\rightarrow X$ from our independence tests is the correct one and thus we can formulate the following output function as the second step in our modified algorithm:

$$dir = \begin{cases} Correct & \text{if } I(X_{Test}, Y_{res}) < \alpha(0.05) \wedge I(Y_{Test}, X_{res}) > \alpha(0.05), \\ Incorrect & \text{otherwise} \end{cases} \quad (3.3)$$

As before, Linear Regression is used. However, for simplicity we only used one independence test: Hilbert-Schmidt Independence Criterion with RBF Kernel (HSIC)³. Here, we use the gamma test to compare the HSIC estimate, that is with the alpha quantile of the gamma distribution with mean and variance of HSIC under independence hypothesis. The HSIC estimator (Gretton et al., 2005) is chosen because of its general good performance in previous results.

3.3.2 Execution

The execution is exactly the same as in Section 3.1.2.

3.3.3 Results

In the following figures the y-axis shows the accuracy ($\frac{\#successful\ tests}{100}$) and the x-axis shows the range of the i factor. Each figure contains two subfigures, the left with $i \in \{0.01, 0.02, \dots, 1.00\}$ and the right figure with $i \in \{1, 2, \dots, 100\}$. Differently from Section 3.1, if HSIC is closer to 0 then we have **unidentifiability**. If plots are closer

³Source: <https://github.com/amber0309/HSIC>

to accuracy 1 then we have very good/consistent **identifiability**. The next subsection describes each figure individually and the subsection thereafter provides a summary and a small conclusion. Additionally, we also directly cover the decoupled estimation together with the coupled estimation approach. Lastly, the figures apply some abbreviations which we shortly explain here:

- GAU: Gaussian distribution.
- UNI: Uniform distribution.
- LAP: Laplace distribution.
- NL***: Non-linear variant.

Furthermore, if in a legend of a plot there are two of the above abbreviations concatenated with a "+", e.g., GAU+UNI, then this signifies that $X \sim \mathcal{N}$ and $N_y \sim \mathcal{U}$ (respecting order). If an abbreviation stands alone, for example GAU, then both variables (X, N_y) are drawn from that distribution.

Individual Analysis

Again, individual analysis can be skipped as we provide a summary in Table 3.3. The following paragraphs describe Fig. 3.38 - Fig. 3.41 which show the performance of using decoupled estimation with a split of 80%/20%. Fig. 3.38 shows all cases where both X and N_y are drawn from the same distribution. $Y = \mathcal{N} + \mathcal{N}$ is the only case which never achieves identifiability with $i \in [0.01; 100]$. The non-linear cases are pretty robust for $i \in [0.2; 1]$; NLLAP remains above 90% accuracy for $i \in [0.3; 100]$ and NLGAU remains over 90% accuracy for $i \in [0.25; 35]$. However, NLUNI already drops fast for $i > 2$ but remains above 90% accuracy for $i \in [0.12; 2]$. UNI and LAP are over 80% accuracy for $i \in [0.5; 2]$ but drop then fast after $i = 2$. Fig. 3.39 shows all cases where $X \sim \mathcal{N}$ and $N_y \not\sim \mathcal{N}$. GAU+UNI only reaches an accuracy of 90% when $i = 2$. GAU+LAP never reaches over 90% accuracy but remains partially over 80% for $i \in [0.6; 1]$. NL_GAU+UNI has an accuracy over 90% for $i \in [0.3; 65]$ and NL_GAU+LAP has also a good accuracy for $i \in [0.2; 20]$.

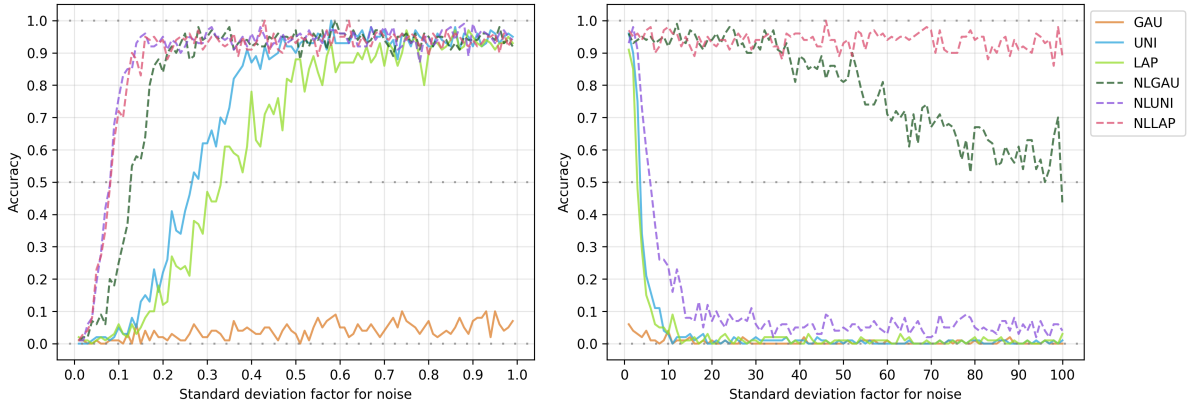


Figure 3.38: $Y = X + N_y$. Contains all cases where X and N_y are drawn from the same type of distribution. Dashed lines are non-linear cases. Decoupled estimation (80% split).

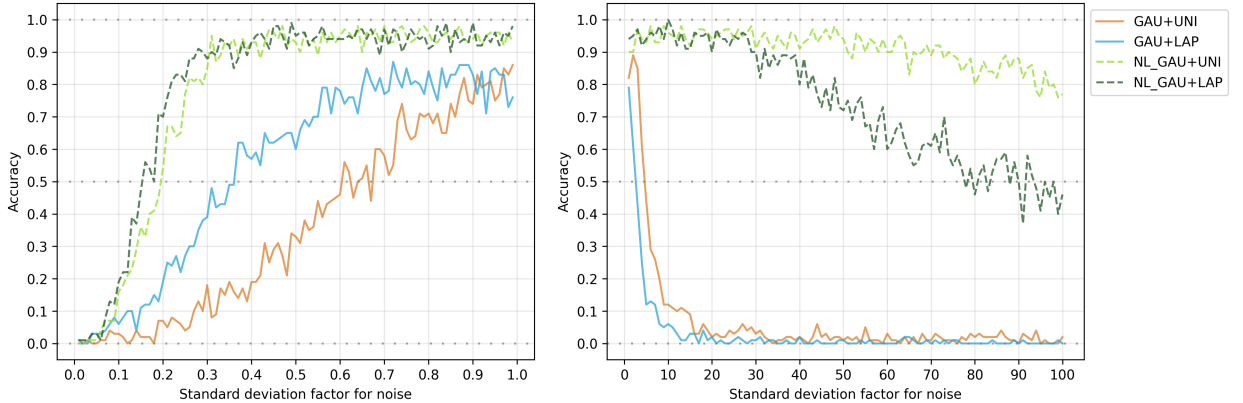


Figure 3.39: $Y = X + N_y$. Contains all cases where $X \sim \mathcal{N}$ and $N_y \not\sim \mathcal{N}$. Dashed lines are non-linear cases. Decoupled estimation (80% split).

Fig. 3.40 shows all cases where $X \sim \mathcal{U}$ and $N_y \not\sim \mathcal{U}$. All cases drop fast to $< 10\%$ accuracy for $i > 1$. NL_UNI+GAU and NL_UNI+LAP are over 90% accuracy for $i \in [0.1; 1]$. UNI+LAP hangs around 90% accuracy for $i \in [0.2; 1]$ and UNI+GAU never reaches a consistent accuracy above 90%, only over 80% for $i \in [0.33; 0.9]$. Fig. 3.41 shows all cases where $X \sim \mathcal{L}$ and $N_y \not\sim \mathcal{L}$. NL_LAP+GAU performs the best here with accuracy above 90% for $i \in [0.3; 100]$, followed by NL_LAP+UNI for $i \in [0.5; 100]$. LAP_UNI only reaches 90% accuracy around $i = 1$. LAP+GAU never $> 90\%$, only 80% for $i \in [0.95; 1]$.

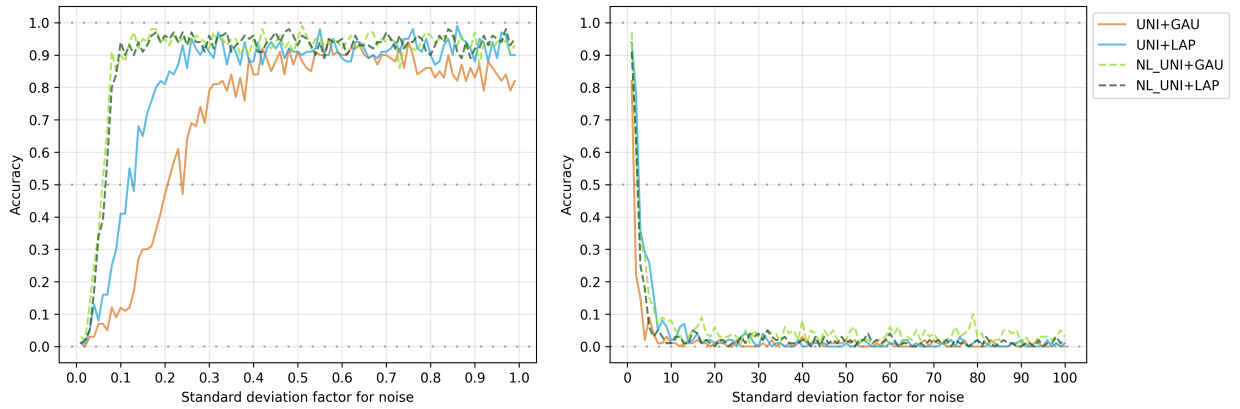


Figure 3.40: $Y = X + N_y$. Contains all cases where $X \sim \mathcal{U}$ and $N_y \not\sim \mathcal{U}$. Dashed lines are non-linear cases. Decoupled estimation (80% split).

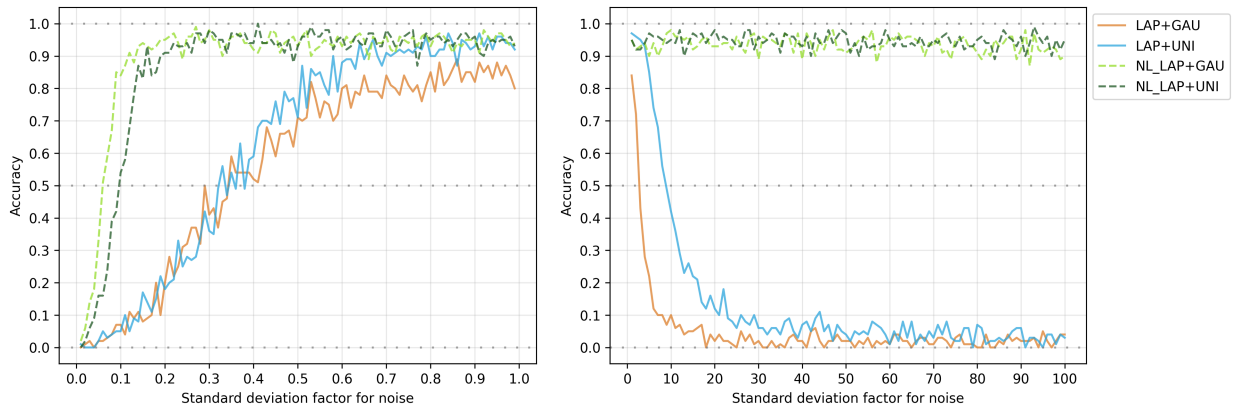


Figure 3.41: $Y = X + N_y$. Contains all cases where $X \sim \mathcal{L}$ and $N_y \not\sim \mathcal{L}$. Dashed lines are non-linear cases. Decoupled estimation (80% split).

The next paragraphs describe Fig. 3.42 - Fig. 3.45 which show the performance of using coupled estimation. Only differences to the decoupled estimation counter part will be described. Fig. 3.42 shows all cases where both X and N_y are drawn from the same distribution. For $i < 1$ all cases (except Gaussian noise only) reach over 90% accuracy earlier, $i \in [0.08; 1]$ for the non-linear equation models and $i \in [0.2; 1]$ for the UNI and LAP models. Furthermore, NLGAU drops more slowly for higher i . Fig. 3.43 shows all cases where $X \sim \mathcal{N}$ and $N_y \not\sim \mathcal{N}$. For $i < 1$ all cases reach over 90% accuracy earlier. Also both linear models now reach an accuracy over 90%, for $i \in [0.25; 5]$ (GAU+LAP) and for $i \in [0.4; 7]$ (GAU+UNI). Both non-linear equation models drop more slowly now for higher i .

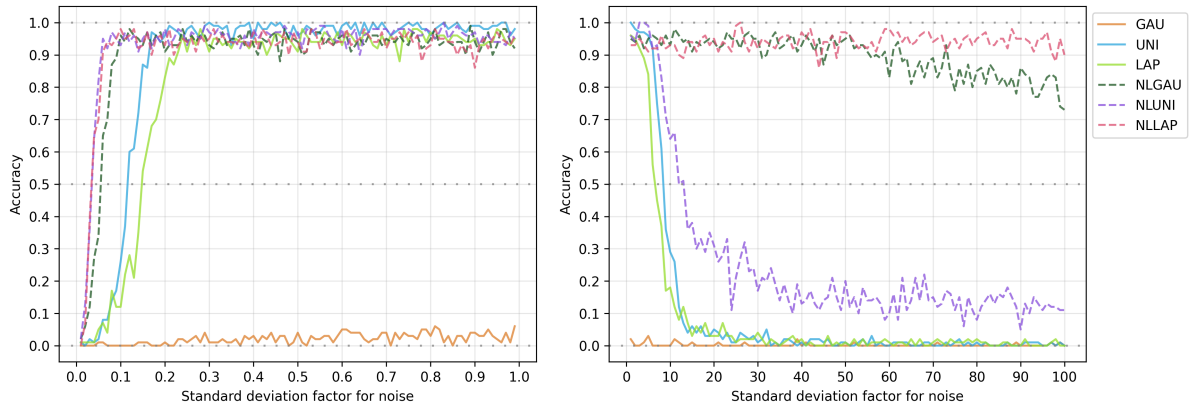


Figure 3.42: $Y = X + N_y$. Contains all cases where X and N_y are drawn from the same type of distribution. Dashed lines are non-linear cases. Coupled estimation.

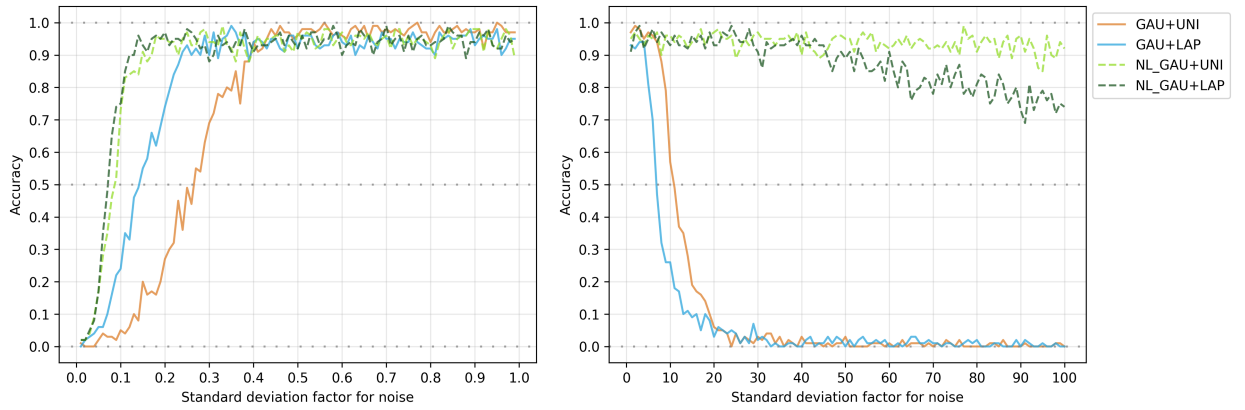


Figure 3.43: $Y = X + N_y$. Contains all cases where $X \sim \mathcal{N}$ and $N_y \not\sim \mathcal{N}$. Dashed lines are non-linear cases. Coupled estimation.

Fig. 3.44 shows all cases where $X \sim \mathcal{U}$ and $N_y \not\sim \mathcal{U}$. For $i < 1$ all cases reach over 90% accuracy earlier. However, both linear equation models show the strongest improvement and have now a consistent accuracy over 90% for $i \in [0.1; 1]$. Fig. 3.45 shows all cases where $X \sim \mathcal{L}$ and $N_y \not\sim \mathcal{L}$. For $i < 1$ all cases reach over 90% accuracy earlier. Again, both linear equation models show the strongest improvement and have now a consistent accuracy over 90% for $i \in [0.25; 1]$.

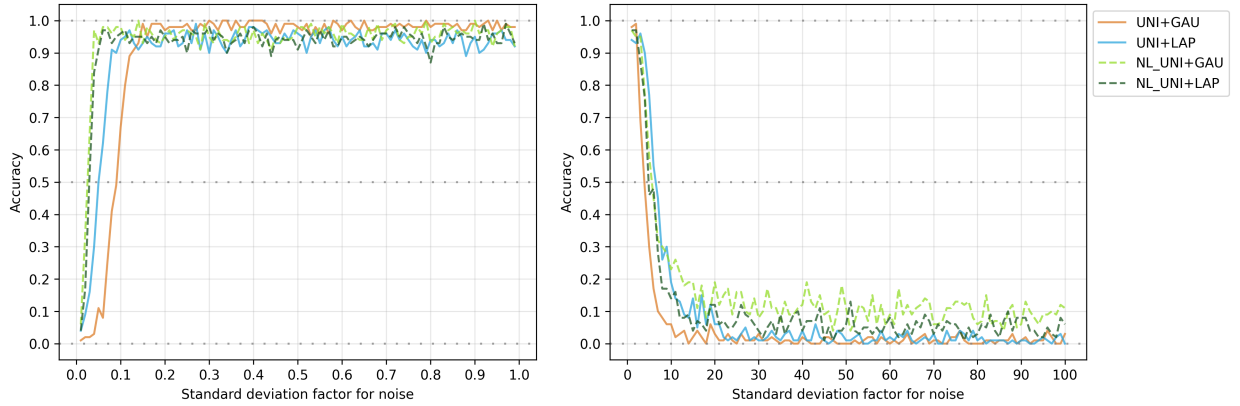


Figure 3.44: $Y = X + N_y$. Contains all cases where $X \sim \mathcal{U}$ and $N_y \not\sim \mathcal{U}$. Dashed lines are non-linear cases. Coupled estimation.

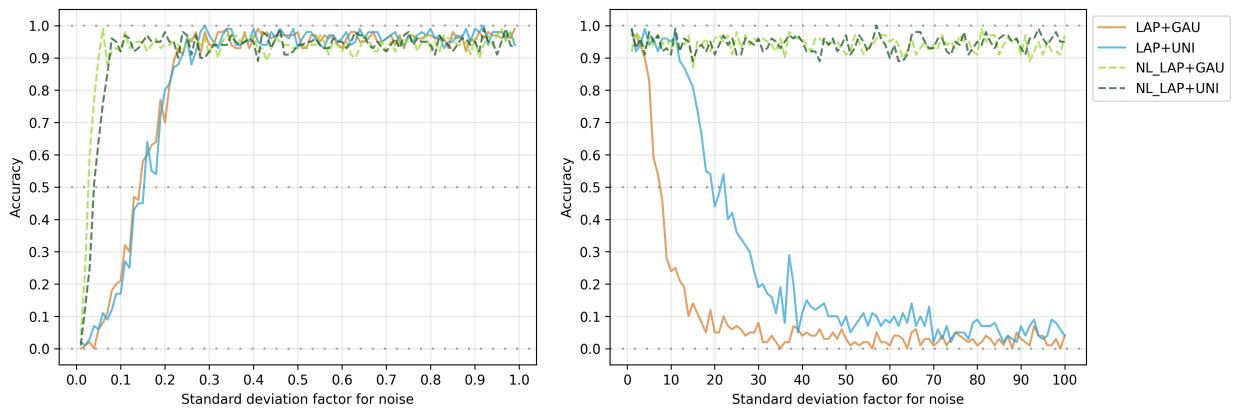


Figure 3.45: $Y = X + N_y$. Contains all cases where $X \sim \mathcal{L}$ and $N_y \not\sim \mathcal{L}$. Dashed lines are non-linear cases. Coupled estimation.

Summary and Conclusion

Table 3.3 follows the same scheme as Table 3.1. However, columns designate decoupled and coupled estimation instead. In general, non-linear cases are often better identifiable than the linear cases. Our results show the differences quite well and further confirm that *"nonlinearities in the data-generating process are in fact a blessing rather than a curse"* - Hoyer et al. (2009). Without the prior assumption models can be well identifiable but are also affected by different noise levels. Also note that in the decoupled estimation we used only 200 samples in the independence test, whereas in the coupled estimation we used the entire set consisting of 1000 samples. For independence tests this can make a difference when considering computation time. Additionally, the changes in terms of improvement between decoupled and coupled estimations are bigger in linear equation models than in non-linear structural causal models. Therefore, for linear structural equations we

generally advise against decoupled estimation, and for non-linear structural equations decoupled estimation can almost always be considered. Again, the biggest advantage of decoupled estimation is lesser computation time, and if the difference of computation time between decoupled and coupled estimation is not significant, then we suggest to go with coupled estimation.

Combinations	Decoupled	Coupled
GAU		
UNI	0.38 - 3	0.16 - 6
LAP	0.57 - 2	0.23 - 4
NLGAU	0.21 - 37	0.09 - 74
NLUNI	0.14 - 4	0.05 - 7
NLLAP	0.13 - 100	0.05 - 100
GAU+UNI		0.39 - 7
GAU+LAP		0.24 - 4
NL_GAU+UNI	0.3 - 74	0.15 - 100
NL_GAU+LAP	0.28 - 33	0.12 - 60
UNI+GAU	0.42 - 0.84	0.13 - 3
UNI+LAP	0.24 - 1	0.07 - 4
NL_UNI+GAU	0.08 - 1	0.04 - 4
NL_UNI+LAP	0.09 - 1	0.05 - 3
LAP+GAU		0.23 - 4
LAP+UNI	0.64 - 4	0.24 - 12
NL_LAP+GAU	0.12 - 100	0.05 - 100
NL_LAP+UNI	0.15 - 100	0.07 - 100

Table 3.3: Summary Table for RESIT & different noise levels & Coupled estimation. The numbers reflect the ranges of noise that allow identifiability with accuracy around 90%.

3.4 RESIT with different means

One question which emerged was how different means for the variables in the equation of additive noise models have an impact on the outcome of the RESIT method. In the previous experiments (Section 3.1 and Section 3.3), we always used linear regression which is computational wise very cheap and showed very good results in linear and non-linear structural causal models. Many recent scientific papers state that any regression method can be used and explicitly or implicitly indicate that means of 0 are assumed in the data (both artificial and natural data). Although, from a mathematical point of view one can already guess that for linear equations there should be no difference and for the non-linear equations identifiability might only be observable around 0 mean for the X variable. Nonetheless, we conducted a range of experiments to analyze how different means for the noise term have an impact on the outcome of RESIT. Again, we have two scenarios, the first one with the prior assumption we made in Section 3.1 (that is only one causal direction must be present in the bivariate case) and the second scenario without this assumption.

3.4.1 Setup

The setup here is a bit different than in Section 3.1.1. For all empirical tests we generate data following $X \rightarrow Y$ and generate linear as well as non-linear cases for each test. Thus, we have the following structural causal model:

$$Y = \beta X + N_y$$

$$(Y = \beta X^3 + N_y \text{ for the non-linear case})$$

where

$$\beta = 1,$$

and

$$X \sim \begin{cases} \mathcal{N}(\mu_X, 1) & \text{or} \\ \mathcal{U}(\mu_X - 1, \mu_X + 1) & \text{or} \\ \mathcal{L}(\mu_X, 1) \end{cases}$$

and

$$N_y \sim \begin{cases} \mathcal{N}(\mu_N, 1) & \text{or} \\ \mathcal{U}(\mu_N - 1, \mu_N + 1) & \text{or} \\ \mathcal{L}(\mu_N, 1) \end{cases}$$

where $\mu_X, \mu_N \in \{-100, -90, -80, \dots, 100\}$. Note that standard deviation (range between lower and upper bound in the uniform case) for both variables are the same. This equals the case where $i = 1$ which showed one of the best results in Section 3.1 and in Section 3.3 so we focus only on these cases for this experiment setup. The algorithm used is the same as in Section 3.1 and we also make use of linear regression and the 12 estimators introduced under Section 3.1.1.

3.4.2 Execution

As previously mentioned, the means μ_X and μ_N are drawn from a set of 21 values:

$$\mu_X, \mu_N \in \{-100, -90, -80, \dots, 100\}$$

Thus we have 441 different combinations and for each combination a linear and a non-linear model of different combinations of distribution types have been tested (18 in total, these are again the same as in Section 3.1.2).

3.4.3 Results

In the following figures the y-axis shows the accuracy ($\frac{\text{\#successful tests}}{100}$) and the x-axis shows all possible combinations of the means for the X and N_y variable, in the following form: μ_X/μ_N . If plots of the estimators are close to 0.5 accuracy then this means that in 50% of the tests the algorithm decided the correct direction (and vice versa 50% the wrong direction) and thus indicates **unidentifiability**. If plots are closer to accuracy 1 then we have very good/consistent **identifiability**. This time we will not cover each individual model because our results confirmed that there is no change at all in terms of accuracy, and results are showing that if μ_X is significantly different from 0 then for non-linear cases the models becomes unidentifiable.

Individual analysis

Fig. 3.46 contains two linear models: on the left we have $Y = \mathcal{N} + \mathcal{U}$ and on the right $Y = \mathcal{U} + \mathcal{L}$. Now if we compare them to Fig. 3.3 and Fig. 3.10, for $i = 1$, respectively, we can see that all estimators remain at the same accuracy. Fig. 3.47 contains two non-linear models: on the left we have $Y = \mathcal{U}^3 + \mathcal{U}$ and on the right $Y = \mathcal{U}^3 + \mathcal{N}$. For both models if $\mu_X = 0 \wedge \mu_N \in [-100; 100]$ then we have identifiability and otherwise the models are unidentifiable as expected. However, in the left model HSIC_IC only reaches $\sim 80\%$ accuracy and for the right model HSIC_IC does not achieve identifiability at all, same as in Fig. 3.11 and Fig. 3.12, respectively.

Summary and Conclusion

As expected the causal relationship directions are recoverable for the linear case on the entire test range for the means. However, for the non-linear case the relationship directions are only recoverable for $\mu_X = 0$. Furthermore, for the non-linear case the estimators HSIC_IC and HSIC_IC2 perform badly, similar to the previous results (see Tables 3.1 to 3.3).

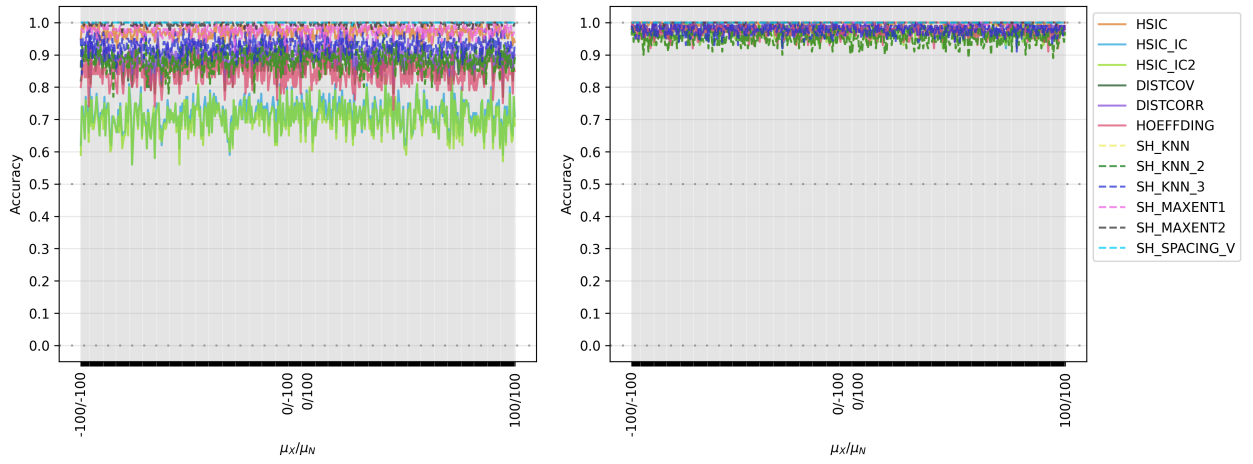


Figure 3.46: Left: $X \sim \mathcal{N}, N_y \sim \mathcal{U}$. Right: $X \sim \mathcal{U}, N_y \sim \mathcal{L}$.

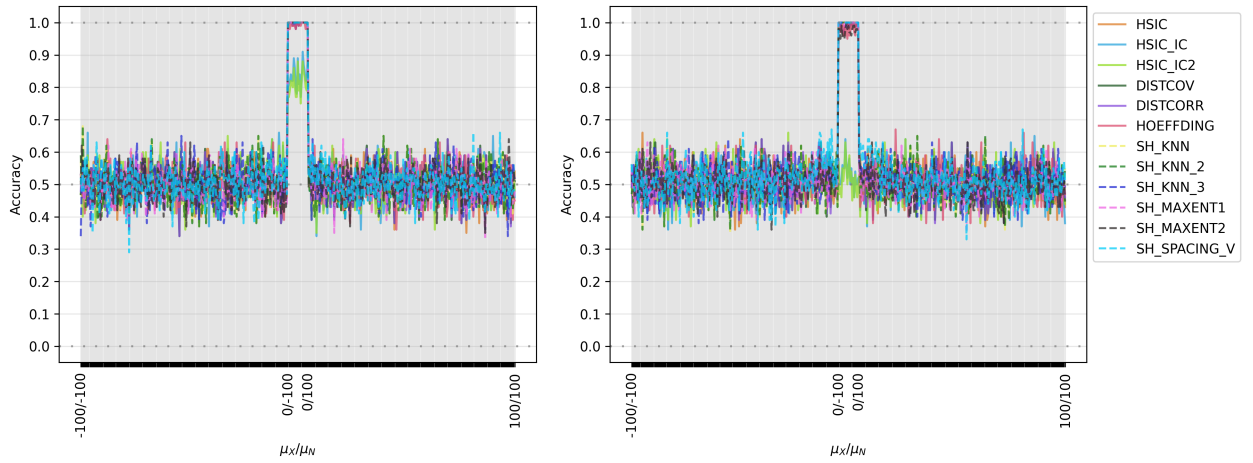


Figure 3.47: Left: $X \sim \mathcal{U}^3, N_y \sim \mathcal{U}$. Right: $X \sim \mathcal{U}^3, N_y \sim \mathcal{N}$.

Chapter 4

Experiments on Identification using Conditional Variances

As already mentioned in Section 3.1.2 the problem of the identifiability of the linear Gaussian structural equation model has only been recently tackled successfully. Peters and Bühlmann (2013), Loh and Bühlmann (2013) and Ghoshal and Honorio (2017) proved that Gaussian linear structural equation models with equal or known error variances are identifiable, and Ghoshal and Honorio (2018) and Chen, Drton, and Wang (2019) proved that Gaussian linear structural equation models with unknown heterogeneous error variances can be identifiable. In this chapter, we will discuss and test the algorithm of Park and Kim (2019) and Park (2020) on bivariate additive noise models, which proved the identifiability of Gaussian structural equation models with both homogeneous and heterogeneous unknown error variances.

4.1 Introduction

Let

$$G_1 : Y = \beta X + N_Y$$

$$G_2 : X = \beta Y + N_X$$

$$G_3 : X = N_X \text{ and } Y = N_Y$$

be the three possible structural equation models for any bivariate additive noise models (acyclic). For G_1 Park (2020) states that if the error variance ratio satisfies $\frac{\text{Var}(Y)}{\text{Var}(X)} > (1 - \beta^2)$ then from the law of total variance we have the following two conditions:

$$(A) \text{Var}(Y) = \mathbb{E}(\text{Var}(Y|X)) + \text{Var}(\mathbb{E}(Y|X)) = \text{Var}(Y) + \beta^2 \text{Var}(X) > \text{Var}(X)$$

$$(B) \mathbb{E}(\text{Var}(X|Y)) = \text{Var}(X) - \text{Var}(\mathbb{E}(X|Y)) \\ = \text{Var}(X) - \frac{\beta^2 \text{Var}(X)^2}{\beta^2 \text{Var}(X) + \text{Var}(Y)} < \text{Var}(Y) = \mathbb{E}(\text{var}(Y|X))$$

For (A) the intuition here is that the level of uncertainty of X is lower than the level of uncertainty of Y since X has only one random source and Y has two random sources. For (B) the intuition is that after eliminating the other variable effect the level of uncertainty of X is smaller than the level of uncertainty of Y . This is because after eliminating the

effect of X the remaining part of Y is N_Y and when eliminating the effect of Y on X the remaining part is $N_X (= X)$ since Y contains some information of N_X . Therefore, one can order the observed variables and one can always recover the true ordering as long as $\frac{Var(Y)}{Var(X)} > (1 - \beta^2)$, even if the error variances are different.

In the same fashion, one can find the true ordering for G_2 as long as $\frac{Var(X)}{Var(Y)} > (1 - \beta^2)$. For the last structural equation model G_3 , we have no guarantee which marginal or conditional variance is bigger and therefore any ordering is considered correct.

Lastly, after determining the orderings for each graph, we simply need to test for the presence of an edge by verifying the dependence relationships between variables. For the graphs G_1 and G_2 , the variables X and Y are dependent and for the graph G_3 the variables are independent. Thus one can recover the true graphs.

4.1.1 Algorithm

The algorithm used for the experiments in this work is composed of Algorithm 2 and Algorithm 3 from Park (2020). As previously hinted, the algorithm is composed of two parts: 1) ordering and 2) conditional independence testing.

1) Ordering - *Backward step wise selection*

For the ordering step the paper Park (2020) proposes two algorithms (Algorithm 1 and 2 from Park (2020)):

Theorem 2 (Identifiability Conditions for ANMs) *Let $P(X)$ be generated from an Additive Noise Model with directed acyclic graph G and true ordering π . Suppose that causal minimality holds. Then, G is uniquely identifiable if either of the two following conditions is satisfied: For any node $j = \pi_m \in V, k \in De(j)$, and $l \in An(j)$,*

$$(A) \text{ Forward step wise selection: } \sigma_j^2 < \sigma_k^2 + \mathbb{E}(Var(\mathbb{E}(X_k|X_{Pa(k)})|X_{\pi_1}, \dots, X_{\pi_{m-1}}))$$

, or

$$(B) \text{ Backward step wise selection: } \sigma_j^2 > \sigma_l^2 - \mathbb{E}(Var(\mathbb{E}(X_l|X_{\pi_1}, \dots, X_{\pi_m} \setminus X_l)|X_{Pa(l)}))$$

For (A) an additive noise model is identifiable if the conditional variance of a node j is smaller than that of its descendant, $De(j)$, given the non-descendants, $Nd(j)$. This can be understood that the variance of N_j is overestimated owing to lack of parents. For (B) an additive noise model is identifiable if the conditional variance of a node j given its parents, $Pa(j)$, is bigger than that of its ancestor, $An(j)$, given the union of its parents and any of its descendants.

In this work we used *Backward step wise selection* (Algorithm 2) as it was more convenient to implement in Python. First we have our set S which contains all nodes from the additive noise model. We iterate over this set S and for each node we calculate its conditional variance given all other remaining nodes in the set S . We select the node with the highest conditional variance and append it to the ordering π and also remove it from the set S . With the updated set S we repeat the process of finding the node with the highest conditional variance, append it to the ordering π and remove it from S . This is repeated until S is empty. Lastly, the *reverse* of the ordering π is returned. (The first node to be appended to the ordering is actually the last one in the ordering, therefore "*backward step wise selection*" is used).

2) Uncertainty Scoring

The second step consists of the uncertainty scoring (Algorithm 3). Here, we iterate over the ordering π and for each node j we perform conditional independence tests with each other node l appearing before node j in the ordering π . If any node l is dependent on j , then we add node l to $\text{Pa}(j)$. Here, the first node in the ordering never has a parent and we start the iteration at the second node in the ordering. For the conditional independence test, Fisher's z-transform of the partial correlation is used. In the following sections we refer to this algorithm as Park algorithm or simply Park.

Algorithm 2 Backward step-wise selection

- 1: **Input:** All variables from an ANM: $X = (x_1, x_2, \dots, x_n)$
 - 2: **Output:** Estimated ordering $\pi = (\pi_1, \pi_2, \dots, \pi_n)$
 - 3:
 - 4: **Procedure**
 - 5: Set $S = \{1, 2, \dots, n\}$
 - 6: List $\pi = []$
 - 7: **for** $m = 1 \dots n$ **do**
 - 8: **for** $j \in S$ **do**
 - 9: Estimate the conditional variance x_j given $\{x_1, \dots, x_n\} \setminus x_j, \sigma_{j|S \setminus j}^2$
 - 10: **end**
 - 11: Append $\pi_m = \text{argmax}_j \sigma_{j|S \setminus j}^2$ to π
 - 12: Update $S = S \setminus \pi_m$
 - 13: **end**
 - 14: Reverse list π
-

Algorithm 3 Uncertainty Scoring

- 1: **Input:** All variables from an ANM: $X = (x_1, x_2, \dots, x_n)$
 - 2: **Output:** Dictionary with estimated parents for all variables: $G = \{Pa(x_1) : [\dots], Pa(x_2) : [\dots], \dots, Pa(x_n) : [\dots]\}$
 - 3:
 - 4: **Procedure**
 - 5: 1) Get ordering from backward step-wise selection:
 - 6: $\pi = (\pi_1, \pi_2, \dots, \pi_n)$
 - 7:
 - 8: 2) Parents estimation
 - 9: $G = \{\}$
 - 10: **for** $m = 2 \dots n$ **do**
 - 11: $Pa(\pi_m) = []$
 - 12: **for** $j = 1 \dots m - 1$ **do**
 - 13: Conditional independence test between π_m and π_j given $\{\pi_1, \dots, \pi_{m-1}\} \setminus \pi_j$
 - 14: If dependent, include π_j into $Pa(\pi_m)$
 - 15: **end**
 - 16: Insert $Pa(\pi_m)$ into G
 - 17: **end**
-

4.2 Setup

The setup is the same as in Section 3.1.1.

4.2.1 Execution

The execution is the same as in Section 3.1.2 except that we use the Park algorithm instead. Here, when using the Park algorithm the output will be a list of parent sets for all nodes in the additive noise model:

Output: $[(Pa(X), Pa(Y))]$.

A test is then successful if and only if

$$(Pa(X) = \{\}) \wedge (Pa(Y) = \{X\}).$$

4.2.2 Results

In the following figures the y-axis shows the accuracy ($\frac{\# \text{successful tests}}{100}$) and the x-axis shows the range of the i factor. Each figure contains two subfigures, the left with $i \in \{0.01, 0.02, \dots, 1.00\}$ and the right figure with $i \in \{1, 2, \dots, 100\}$. Differently from Section 3.1, if HSIC is closer to 0 then we have **unidentifiability**. If plots are closer to accuracy 1 then we have very good/consistent **identifiability**. The next subsection describes each figure individually and the following subsection thereafter provides a summary and a small conclusion.

Individual Analysis

Fig. 4.1 shows the results for all linear cases. For $i \in [0.5; 3]$ all linear structural equation models are always identifiable. For $i < 0.5$ all models slowly drop towards 50% accuracy. For $i > 3$ all cases start dropping in terms of accuracy. Some do drop faster (UNIxLAP, UNIxGAU, GAUxLAP, GAU, UNI, LAP) and others more slowly (LAPxGAU, GAUxUNI, LAPxUNI). For $i > 5$ the first case (UNIxLAP) is below 90% accuracy and for $i > 25$ all cases are below 90% accuracy.

Fig. 4.2 shows the results for non-linear cases. Here, the results are quite different and varying. NL_UNIxLAP, NL_UNIxGAU and NLUNI have accuracy 100% for $i \in [0.12; 1]$. After $i = 1$ they drop fast below 50% accuracy. NLGAU and NL_GAUxLAP reach an accuracy over 90% for $i \in [0.35; 25]$ and slowly drop outside this range in terms of accuracy. NL_GAUxUNI has accuracy over 90% for $i \in [0.77; 58]$ and slowly drops outside this range. The last three, NLLAP, NL_LAPxGAU and NL_LAPxUNI only reach an accuracy higher than 90% for $i \in [3; 100]$.

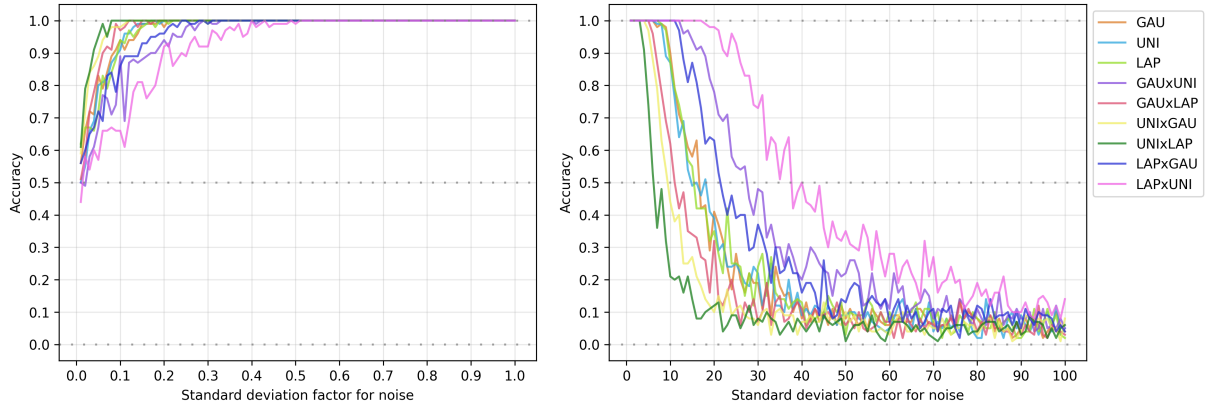


Figure 4.1: $Y = X + N_y$. Contains all linear cases.

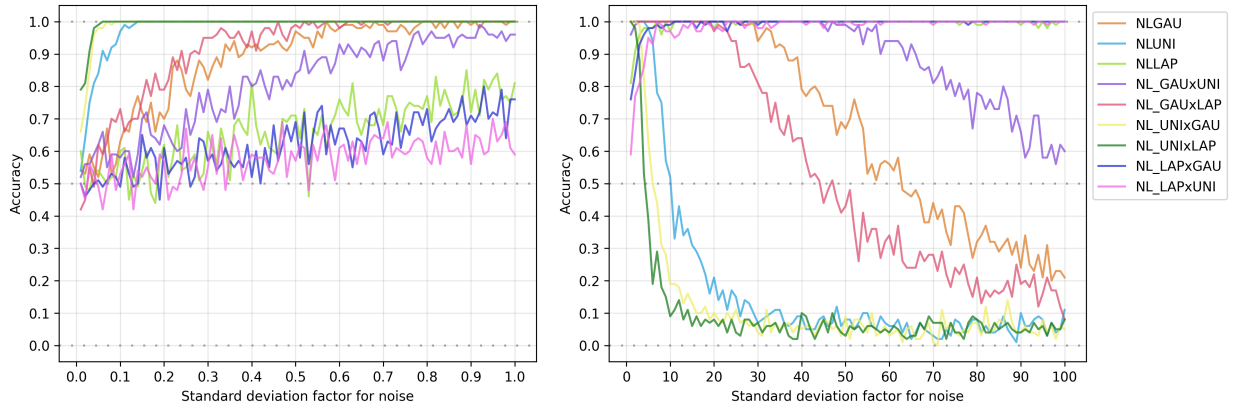


Figure 4.2: $Y = X^3 + N_y$. Contains all non-linear cases.

Summary and Conclusion

Table 4.1 follows the same scheme as Table 3.3. Interestingly, for $i \in [0.01; 1]$ the linear cases perform better than the non-linear cases and for $i \in [1; 100]$ several non-linear cases perform better than most linear cases, which wasn't the case for RESIT. Furthermore, as the results show, after specific noise levels the identifiability from the Park algorithm

starts to suffer and thus not all graphs can be successfully recovered. The reason for this lies within step 2, the conditional independence test. If noise levels are significantly different then the independence test fails to capture the correlation between the two nodes and therefore concludes that the nodes are independent (Type II Error). However, for any given i , the ordering step always performs correctly.¹

Combinations	Coupled
GAU	0.08 - 10
UNI	0.1 - 8
LAP	0.1 - 10
GAU+UNI	0.16 - 10
GAU+LAP	0.05 - 6
UNI+GAU	0.04 - 5
UNI+LAP	0.03 - 3
LAP+GAU	0.14 - 13
LAP+UNI	0.19 - 26
NLGAU	0.33 - 37
NLUNI	0.05 - 6
NLLAP	2 - 100
NL_GAU+UNI	0.52 - 67
NL_GAU+LAP	0.23 - 25
NL_UNI+GAU	0.04 - 4
NL_UNI+LAP	0.03 - 3
NL_LAP+GAU	4 - 100
NL_LAP+UNI	5 - 100

Table 4.1: Summary Table for Uncertainty Scoring & different noise levels & Coupled estimation. The numbers reflect the ranges of noise that allow identifiability with accuracy around 90%.

¹A quick test in python shell, with $i = 57$, $X \sim \mathcal{L}$ and $N_y \sim \mathcal{U}$ and 100 repetitions showed that in these runs the ordering was always correct but only in 35 runs (from the 100 repetitions) the independence tests were correct.

Chapter 5

Conclusion and Future Work

The results from the experiments showed that two analyzed causal discovery methods (RESIT and Uncertainty Scoring) are affected by different noise scales. For significantly small noise levels in the disturbance term N_y (almost deterministic data), or significantly high noise levels, these causal discovery methods fail to capture the true causal relationship of the given structural equation model. Recall that *significantly* here depends on the model. For example, on some models if the noise level was already twice larger then the methods failed to determine the causal direction consistently. Other models remained identifiable with 100 times higher noise levels (The range of different noise levels in the experiments was quite exhaustive, and realistically speaking having noise levels 100 times higher then the potential cause variable is very rare¹). This also shows different behavior for different distribution types (e.g., Gaussian or Uniform). Therefore, if observed data differs significantly in terms of variances scientists need to be careful when analyzing causal relationships and in drawing conclusions.

In Chapter 3 we tested RESIT in the bi-variate case using several estimators (12 in total). We compared decoupled estimation (splitting data into training and test data) and coupled estimation (no splitting) in Section 3.1 and Section 3.2. In Section 3.3 we omitted a particular assumption which allowed us to use entropy estimators and therefore restricted our setting in using only independence tests. All results from these sections are quite similar. In general, if the standard deviation of the noise term is smaller than the standard deviation of the cause then models remained identifiable as opposed to the case when the standard deviation of the noise term was bigger. For example, often when the standard deviation of the noise term was only half of that of the cause, the model was still identifiable. However, in several cases, if the standard deviation of the noise term was already twice larger than the standard deviation of the cause, then the model became unidentifiable. We also tested linear and non-linear models and our results show that non-linear models were still identifiable in situations where a linear model were unidentifiable. For example, some non-linear models, where the noise term's standard deviation was 100 times higher than that of the cause, were still perfectly identifiable while their linear counterpart wasn't. Similar results can be observed in the Uncertainty Scoring method (Chapter 4).

Specific to RESIT, we also tested whether splitting data into training and test data was beneficial. The reason to do this is to use only the test data in the estimators and therefore reduce the overall computation time of the algorithm. Hence, we analysed the

¹Additionally, with very high noise levels the effect of the cause variable is very likely negligible anyways

identifiability performance between decoupled estimation and coupled estimation. Our results show that there is a performance drop from coupled to decoupled estimation. However, in linear cases, this drop is bigger than in non-linear cases. Also, our results show that decoupled estimation for non-linear cases has almost no significant impact on the performance of RESIT. For linear models we generally advise to use coupled estimation. In the end this is a trade-off between performance and computation speed and should be carefully selected depending on the individual experiment. Lastly, for RESIT we used several estimators (6 independence estimators and 6 entropy estimators). Our results show differences in terms of performance in these estimators. In our experiments Hilbert-Schmidt Independence Criterion with RBF Kernel was the best independence estimator, and Shannon entropy estimator using Vasicek's spacing method was the best entropy estimator.

Future work. In our experiments, we tested only two particular methods and three different distribution types. Similar results are expected with other methods for causal discovery for additive noise models, as the failing point is the independence estimation (or entropy estimation) in the two used methods. Therefore, methods relying on these estimations are generally prone to errors for some levels of noise. Furthermore, this work does not formalize the effect of different noise levels in ANM causal discovery methods but could be done in a future work.

In reality, observed data does not always strictly follow a certain distribution type. As there are many different combinations possible, it would be interesting to generalize the impact of different noise levels on any distribution by using the different properties an observed distribution exhibits.

Acknowledgement

I want to express my many thanks to Dr. Marharyta Aleksandrova. I enjoyed working on this topic a lot, and I am grateful to have had Dr. Aleksandrova as my advisor. She is a very proactive and professional researcher, and I learned a lot from her. Furthermore, she gave me a lot of feedback on my thesis text, which helped me improve the quality of the thesis text a lot.

Bibliography

- Wright, Sewall (1921). “Correlation and causation”. In: *J. agric. Res.* 20, pp. 557–580.
- Rebane, George and Judea Pearl (2013). “The Recovery of Causal Poly-Trees from Statistical Data”. In: *CoRR* abs/1304.2736. arXiv: 1304.2736. URL: <http://arxiv.org/abs/1304.2736>.
- Spirtes, Peter, Clark Glymour, and Richard Scheines (Jan. 1993). *Causation, Prediction, and Search*. Vol. 81. ISBN: 978-1-4612-7650-0. DOI: 10.1007/978-1-4612-2748-9.
- Spirtes, Peter et al. (2000). *Causation, prediction, and search*. MIT press.
- Judea, Pearl (2000). “Causality: models, reasoning, and inference”. In: *Cambridge University Press*. ISBN 0 521.77362, p. 8.
- Janzing, Dominik et al. (2012). “Information-geometric approach to inferring causal directions”. In: *Artificial Intelligence* 182, pp. 1–31.
- Sgouritsa, Eleni et al. (2015). “Inference of cause and effect with unsupervised inverse regression”. In: *Artificial intelligence and statistics*. PMLR, pp. 847–855.
- Friedman, Nir and Iftach Nachman (2013). “Gaussian Process Networks”. In: *CoRR* abs/1301.3857. arXiv: 1301.3857. URL: <http://arxiv.org/abs/1301.3857>.
- Kano, Yutaka and Shohei Shimizu (2003). “Causal inference using nonnormality”. In: *Proceedings of the international symposium on science of modeling, the 30th anniversary of the information criterion*, pp. 261–270.
- Shimizu, Shohei et al. (2006). “A linear non-Gaussian acyclic model for causal discovery.” In: *Journal of Machine Learning Research* 7.10.
- Shimizu, Shohei, Aapo Hyvarinen, and Yoshinobu Kawahara (2014). *A direct method for estimating a causal ordering in a linear non-Gaussian acyclic model*. arXiv: 1408.2038 [cs.LG].
- Sun, Xiaohai, Dominik Janzing, and Bernhard Schölkopf (2006). “Causal inference by choosing graphs with most plausible Markov kernels”. In: *Ninth International Symposium on Artificial Intelligence and Mathematics (AIMath 2006)*, pp. 1–11.
- (2008). “Causal reasoning by evaluating the complexity of conditional densities with kernel methods”. In: *Neurocomputing* 71.7-9, pp. 1248–1256.
- Hoyer, Patrik et al. (2009). “Nonlinear causal discovery with additive noise models”. In: *Advances in neural information processing systems* 21, pp. 689–696.
- Janzing, Dominik, Patrik O Hoyer, and Bernhard Schölkopf (2009). “Telling cause from effect based on high-dimensional observations”. In: *arXiv preprint arXiv:0909.4386*.
- Mooij, Joris et al. (2009). “Regression by dependence minimization and its application to causal inference in additive noise models”. In: *Proceedings of the 26th annual international conference on machine learning*, pp. 745–752.

- Stegle, Oliver et al. (2010). “Probabilistic latent variable models for distinguishing between cause and effect”. In: *Advances in neural information processing systems* 23, pp. 1687–1695.
- Mooij, Joris M et al. (2011). “On causal discovery with cyclic additive noise model”. In: Zhang, Kun and Aapo Hyvarinen (2012). *On the Identifiability of the Post-Nonlinear Causal Model*. arXiv: 1205.2599 [stat.ML].
- Daniusis, Povilas et al. (2012). “Inferring deterministic causal relations”. In: *arXiv preprint arXiv:1203.3475*.
- Hyvärinen, Aapo and Stephen M Smith (2013). “Pairwise likelihood ratios for estimation of non-Gaussian structural equation models”. In: *Journal of Machine Learning Research* 14.Jan, pp. 111–152.
- Shimizu, Shohei (2014). “LiNGAM: Non-Gaussian methods for estimating causal structures”. In: *Behaviormetrika* 41.1, pp. 65–98.
- Peters, J. and P. Bühlmann (Nov. 2013). “Identifiability of Gaussian structural equation models with equal error variances”. In: *Biometrika* 101.1, pp. 219–228. ISSN: 0006-3444. DOI: 10.1093/biomet/ast043. eprint: <https://academic.oup.com/biomet/article-pdf/101/1/219/17460568/ast043.pdf>. URL: <https://doi.org/10.1093/biomet/ast043>.
- Peters, Jonas et al. (2014). “Causal discovery with continuous additive noise models”. In: Nowzohour, Christopher and Peter Bühlmann (2016). “Score-based causal learning in additive noise models”. In: *Statistics* 50.3, pp. 471–485.
- Park, Gunwoong and Younghwan Kim (2019). *Identifiability of Gaussian Structural Equation Models with Homogeneous and Heterogeneous Error Variances*. arXiv: 1901.10134 [stat.ML].
- Chen, Wenyu, Mathias Drton, and Y Samuel Wang (2019). “On causal discovery with an equal-variance assumption”. In: *Biometrika* 106.4, pp. 973–980.
- Kpotufe, Samory et al. (2014). “Consistency of causal inference under the additive noise model”. In: *International Conference on Machine Learning*. PMLR, pp. 478–486.
- Park, Gunwoong (2020). “Identifiability of Additive Noise Models Using Conditional Variances.” In: *Journal of Machine Learning Research* 21.75, pp. 1–34.
- Mooij, Joris M et al. (2016). “Distinguishing cause from effect using observational data: methods and benchmarks”. In: *The Journal of Machine Learning Research* 17.1, pp. 1103–1204.
- Cover, Thomas M (1999). *Elements of information theory*. John Wiley & Sons.
- Szabó, Zoltán (2014). “Information Theoretical Estimators Toolbox”. In: *Journal of Machine Learning Research* 15, pp. 283–287.
- Gretton, Arthur et al. (2005). “Measuring statistical dependence with Hilbert-Schmidt norms”. In: *International conference on algorithmic learning theory*. Springer, pp. 63–77.
- Loh, Po-Ling and Peter Bühlmann (2013). *High-dimensional learning of linear causal networks via inverse covariance estimation*. arXiv: 1311.3492 [stat.ML].
- Ghoshal, Asish and Jean Honorio (2017). “Learning identifiable gaussian bayesian networks in polynomial time and sample complexity”. In: *arXiv preprint arXiv:1703.01196*.

- (2018). “Learning linear structural equation models in polynomial time and sample complexity”. In: *International Conference on Artificial Intelligence and Statistics*. PMLR, pp. 1466–1475.